

**MATHEMATICAL MODELS OF THE ADAPTIVE
IMMUNE RESPONSE IN A NOVEL CANCER
IMMUNOTHERAPY**

by

Bryan A. Dawkins

A dissertation submitted to the faculty of
The University of Central Oklahoma
in partial fulfillment of the requirements for the degree of

Master of Science

Department of Mathematics

The University of Central Oklahoma

May 2016

Copyright © Bryan A. Dawkins 2016

All Rights Reserved

THE UNIVERSITY OF CENTRAL OKLAHOMA GRADUATE SCHOOL

SUPERVISORY COMMITTEE APPROVAL

of a dissertation submitted by

Bryan A. Dawkins

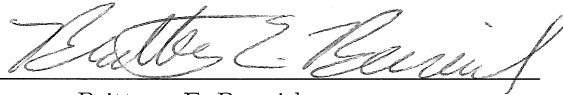
This dissertation has been read by each member of the following supervisory committee and by majority vote has been found to be satisfactory.

4-28-2016



Chair: Sean M. Lavery

4/28/16



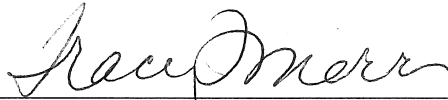
Brittany E. Bannish

April 28 2016



Wei R. Chen

4/29/16



Tracy L. Morris

ABSTRACT

The immune system is the first line of defense against cancer. The immune system regularly detects and destroys cancer cells. Despite this continuous protection, certain cancers are able to escape detection or destruction by the immune system. Research in recent decades has addressed the possibility of enlisting the help of the immune system to detect and destroy cancer cells. One compelling treatment uses a laser, an immune stimulant called glycated chitosan (GC), and a light absorbing dye called indocyanine green to convince the immune system to incite a systemic attack against both primary and metastatic tumors. In successful treatments, all tumors are completely destroyed and patients develop long-term immunity against tumors. While attempting to locate and destroy tumor cells, the cells of the immune system face competing pressures. On one hand are the immune cells that detect and attempt to control tumor cells (typically the target of the immune response is a foreign invader), and on the other hand are the immune cells that prevent the response from growing dangerously out of control. By policing certain immune cell populations, regulatory T cells (Tregs) play an important role in keeping the overall immune response under control. But, in doing so, these Tregs indirectly protect cancer cells.

We describe post-treatment immune dynamics with mathematical models, and predictions of clinical treatment outcomes can be drawn from model predictions. Currently we emphasize the role of cytotoxic T cells and dendritic cells in the laser-initiated immune response, but we have also studied the roles of B cells and helper T cells. Our model is based on experimental studies with the dimethylbenza(a)anthracene-4 (DMBA-4) metastatic mammary tumor line in the rat animal model. We have used our model to determine clinical outcomes based on the effects of two key treatment factors: the dose and role of GC, and the manipulation of Treg activity. Treatment outcome is improved by the pro-immune stimulatory properties of GC and worsened by the proposed pro-tumor activity of Tregs. The results from our studies indicate potential treatment designs that could be used to improve treatment outcome or highlight additional areas that should be targeted for future experimentation with animal models.

I would like to dedicate this to my family and my wonderful wife. You have all been instrumental in my development into the person I am today.

CONTENTS

ABSTRACT	ii
LIST OF FIGURES	vi
LIST OF TABLES	vii
ACKNOWLEDGEMENTS	viii
CHAPTERS	
1. INTRODUCTION	1
1.1 Cancerous Tumor Growth	1
1.2 Cancer Immunotherapies	2
1.3 Mathematical Models of Cancer Immunology	2
1.4 Categories of Immunity	3
1.5 Dendritic Cells (DCs)	3
1.6 T Cells	4
1.6.1 Cytotoxic T Lymphocytes (CTLs)	4
1.6.2 Helper T Cells	4
1.6.3 Regulatory T Cells (Tregs)	4
1.7 B Cells and Antibodies	5
1.8 Immunoadjuvants and Elements of Treatment	5
2. MATHEMATICAL MODEL	6
2.1 Mathematical Model	7
2.2 Parameterization	10
3. ANALYSIS OF MATHEMATICAL MODEL	14
3.1 Sensitivity Analysis	15
3.1.1 Latin Hypercube Sampling	15
3.2 Predictions of Treatment Outcomes	17
3.3 Modeling the Effects of Glycated Chitosan (GC)	21
3.4 Regulatory T Cell Experimental Simulation	24
4. DISCUSSION	29
4.1 Summary	29
4.2 Suggested experiments	30

5. FUTURE WORK	32
5.1 Modeling	32
5.2 Experimentation	32
5.3 Speculation	33
APPENDICES	
A. IMMUNOLOGICALLY EXPANDED MODEL	34
B. REDUCED MODEL WITHOUT CTL PROLIFERATION	36
C. MODEL OF CTL PROLIFERATION	37
D. NON MASS-ACTION VS. MASS-ACTION TUMOR CELL KILLING	39
REFERENCES	40

LIST OF FIGURES

2.1	Conceptual model of anti-tumor laser immunotherapy.	6
2.2	Predicted tumor-immune dynamics for successful treatment.	8
2.3	CTL progression through proliferative stages.	9
2.4	Parameters partitioned by innate, cancer, Treg, and GC processes.	11
3.1	Sample stratified parameter distribution.	15
3.2	Comparison of 2D Latin Hypercube and Simple Random Sampling.	16
3.3	(Revisited) Predicted tumor-immune dynamics for successful treatment.	18
3.4	(Revisited) CTL progression through proliferative stages.	20
3.5	Variation in clinical outcomes across patient parameters.	21
3.6	Variation in clinical outcomes across GC parameters.	23
3.7	Model simulation across GC parameters.	24
3.8	Simulated cell dynamics across all clinical outcomes.	26
3.9	Variation in clinical outcomes across Treg activity parameters.	27
C.1	Comparison of CTL dynamics with and without proliferation.	38
D.1	Comparison of tumor dynamics with CTL and without CTL proliferation.	39

LIST OF TABLES

2.1 Patient parameter values, units, and references.	12
2.2 Regulatory T cell, cancer, and glycated chitosan associated parameter values, units, and references.	13
3.1 Sample GC parameters with respect to clinical outcome.	22
3.2 Sample Treg activity parameters with respect to clinical outcome.	28

ACKNOWLEDGEMENTS

- I would like to especially thank my advisor, **Dr. Sean M. Lavery**, for being the reason I started doing research from the beginning of my time at UCO. When I first stepped foot into your differential equations class as a first-semester transfer student, I was a nervous wreck. I was terrified of failure and I never even considered the possibility that I might write and present mathematical models in front of audiences, let alone teach my own students. Even though I desired to do research outside the classroom, I would have never asked anyone because I was too terrified of the idea of possibly being rejected. When you asked me if I would be interested in doing research, you opened the door to personal growth that I would have never achieved on my own. You have given me so many opportunities and you have taught me so much. You have given me advice in every major decision I have had to make in terms of my future direction. My hope is that I will one day be able to make an impact in a student's life like you have impacted mine. I will be forever grateful to you for all you have done for me.
- To **Dr. Brittany E. Bannish**, I would like to thank you for always helping me extend my knowledge by asking difficult questions regarding the work I have done as I have presented it to you. There were many times when you asked me questions I had not yet considered, which led me to dig deeper into the literature or go back to the drawing board so I could figure things out. Thank you for always being encouraging and for giving me much needed advice about graduate school and what to expect as my future unfolds.
- **Dr. Wei R. Chen** and the entire **Biophotonics Research Laboratory** are the reason the topic of my research even exists. I have been fascinated by your work from the first time I initially read one of your published papers. Since then, I have learned so much and I have great appreciation for the complexity of immunological responses to cancer. Thank you for making my research possible.

- I would like to thank **Dr. Charles L. Cooper** for enhancing my appreciation and understanding of mathematics. Thank you for enlightening me on what mathematics is and what it is not. Also, thank you for always challenging your students to think critically to become better problem solvers.
- I would like to thank **Dr. Tracy L. Morris** for being such a hard working, helpful teacher. Thank you for asking questions and offering your help on my project at the late stage it was in.
- Thank you to all of the **Mathematics and Statistics faculty** for being wonderful teachers and for being so involved with your students. The UCO Math and Stat Department is like a family. You all work so well together and it makes the entire operation more effective. You all are what makes the university the wonderful place that it is.
- Without the **RCSA grant program** and **CURE-STEM** at UCO, I would have never been able to do productive research for financial reasons. This program provided me with the time that I needed to accomplish difficult research tasks throughout my entire time at UCO.
- Thank you to my entire family who has supported me throughout my entire life. Thank you to my wonderful wife, Grace, who has been so encouraging and by my side in everything I do.

CHAPTER 1

INTRODUCTION

To begin our work mathematically modeling a potential mechanism underlying a novel anti-tumor immunotherapy, we give a brief introduction to cancerous tumor growth, cancer immunotherapies, existing cancer models, and immunology. The activities of the immune system cells listed are not limited to anti-tumor immunity. However, the descriptions of each cell type will be limited to the proposed role that each cell plays in the anti-tumor laser immunotherapy treatment.

1.1 Cancerous Tumor Growth

Cancerous tumors form when one or more of an organism's cells ceases to operate in accordance with its normal cellular cycle. This can be caused by random mutations in a segment of a cell's DNA that controls for programmed cell death or apoptosis. This can also be caused by a mutation in the segment of DNA that controls cellular division, in which a cell makes a copy of itself [1, 2, 3]. An organism's innate immune system, the cells of its immune system requiring no preliminary activation to combat invaders, constantly surveys its surroundings. When a cancerous cell is recognized, innate cells can kill it [4]. However, when all of these checkpoints have failed to eradicate cancer cells, uncontrolled proliferation and migration of cancer cells can occur. This uncontrolled cancer cell growth can interfere with normal organ function on a scale that can cause the death of an organism. Cancer cell migration, or metastasis, makes the task of curing a patient of cancer much more difficult. An isolated tumor that has not metastasized stays fixed in a single location, so it is easier to locate for treatment. However, when tumor cells branch off a primary tumor and spread to other locations, the act of surgically removing tumors of the primary tumor cell line can be tremendously difficult [1, 2, 3]. This implies that cancer therapies must be able to eradicate tumors in numerous, and possibly unidentifiable, locations.

1.2 Cancer Immunotherapies

There are many types of therapies for cancer aimed at using immune components, termed immunotherapies. Numerous vaccines have been created that have caused significant regression of cancerous tumors in some patients [5, 6]. There are also viral therapies that aim to use oncolytic (cell lysing) viruses to infect and kill tumor cells [7, 8, 9]. This therapy can also indirectly inform the immune system that cancer cells are present due to the fact that a patient's immune system can recognize the presence of viruses [8, 9]. When immune cells recognize that a cancer cell is infected with a virus, they will force the cancer cell into apoptosis to kill the cell [8, 9]. It is also possible to extract a patient's immune cells, train them to fight cancer, and then re-inject them back into the patient. This immune cell extraction and training before re-injection has been shown to be quite effective in treating cervical cancers [10].

Anti-tumor laser immunotherapy is a promising approach to treating cancerous tumors [11, 12, 13, 14, 15, 16, 17, 18]. Laser immunotherapy uses a laser to kill cancer cells, which releases a cancer signal to the immune system, in the form of proteins. With the aid of immune stimulants, this therapy has been shown to be quite effective in treating patients with metastatic tumors [11, 12, 13, 14, 15, 16, 17, 18]. Our focus is the anti-tumor laser immunotherapy performed in the laboratory on rats inoculated with metastatic mammary tumors [15].

1.3 Mathematical Models of Cancer Immunology

The concept of modeling immunological responses to cancer is certainly not new. There is a balance between biological detail and mathematical simplicity when writing models of biological processes. Many models are polarized towards mathematical complexity, and include less explicit treatment for individual immune cells. The more complex mathematical models frequently address three components: an overall cancer or tumor burden, an immune effectivity, and drug or chemical concentration affecting the immune component [19]. This type of model is phenomenological in nature, which makes biological interpretation of variables and parameter units less obvious. However, the limited number of equations in such a model implies fewer unknowns which can make parameter estimation more feasible. Including a more explicit treatment of individual immune cell types makes models more descriptive and easier to explain in a biological context. Increased biological detail implies an increase in the number of variables and model parameters, which is demonstrated in

[20, 21]. These ordinary differential equation models explicitly include components for cancer, several types of immune cells, or immune-affecting chemicals and chemotherapy drugs. One incentive in writing a more biologically descriptive model is that it can be used in a variety of contexts. In such models, one type of treatment can easily be replaced by another to analyze multiple treatment scenarios. Models using immunotherapy and/or chemotherapy of cancer could be altered slightly to incorporate an oncolytic virotherapy model [22].

1.4 Categories of Immunity

The immune system has two major categories: the innate immune system and the adaptive immune system. The innate immune system, named for the fact that it is common among all animals, includes cells that are always actively seeking and destroying invaders that have entered an organism [4]. Innate immunity is the first line of defense against a new threat to an organism [4]. The adaptive immune system, on the other hand, must be activated in order to combat an invader [4]. Adaptive immunity is appropriately called “adaptive” because each threat type will lead to a unique secondary, or adaptive, immune response. The adaptive component of the immune system is capable of remembering a past invader or threat, which means that an organism’s immune system will progressively adapt to the host’s surroundings [4].

1.5 Dendritic Cells (DCs)

The adaptive immune response to cancerous tumors begins with the uptake and processing of tumor antigen, which are the roles of dendritic cells [23, 24, 25, 26, 27, 28, 29]. Tumor antigen consists of tumor cell protein fragments released by laser-induced cellular apoptosis [30]. Laser irradiation of a primary tumor usually lasts for about 10 minutes, which causes the release of tumor antigen to the neighboring tissues and blood [11, 12, 13, 14, 15, 16, 17, 18]. Naive or inactive dendritic cells then take in antigen, which initiates and drives their activation process [23, 24, 25, 26, 31, 27, 28, 32, 29, 33, 34, 35]. The initial stage of activation is one of migration to the surrounding lymph nodes, during which dendritic cells continually process antigen into peptides and load them onto their surface for presentation to naive cytotoxic T cells, helper T cells, and B cells [23, 26, 31, 36, 34, 35]. Upon reaching the lymph nodes, dendritic cells are fully activated and capable of presenting to several naive T and B cells. As long as tumor cell killing is occurring, antigen will

continually be released via tumor cell apoptosis. Therefore, dendritic cells will continue to carry out this process until all tumor cells have been eradicated [11, 12, 13, 14, 15, 16, 17, 18].

1.6 T Cells

T cells perform a variety of tasks after activation via antigen presentation. Each type of T cell has a unique role in the immune response, ranging from killing tumor cells to defending tumor cells [37, 38, 39].

1.6.1 Cytotoxic T Lymphocytes (CTLs)

Before antigen presentation, naive CTLs remain in the lymph nodes [40]. Once antigen is presented to a naive CTL, the cell becomes activated and leaves the lymph node to begin clonal proliferation [41]. In this process, CTLs drastically increase in number in proportion to the severity of the infection (surviving primary and metastatic tumor cells). After proliferation, CTLs travel to all tumor sites to begin infiltrating tumors and killing tumor cells [40]. The lifespan of CTLs will depend on how active they are at the “battle site” [4], how effective immunosuppressive activity is in the tumor microenvironment [42, 43, 44], and whether or not these cells are restimulated by other immune cells [4].

1.6.2 Helper T Cells

Similar to CTLs, helper T cells remain in the lymph nodes in a naive state prior to antigen presentation [45, 4]. Once activated via antigen presenting dendritic cells, helper T cells leave the lymph nodes to proliferate [45, 4]. Unlike CTLs, activated helper T cells are involved in the activation or stimulation of other immune cells [45, 4, 46, 47, 48, 49, 50]. Activated helper T cells have been shown to help CTLs proliferate by releasing a growth factor called interleukin 2 (IL-2) [47, 50, 45, 46, 4]. During B cell-helper T cell contact, activated helper T cells can provide a stimulatory influence on antigen-primed B cells with a type of surface protein called CD40L [4].

1.6.3 Regulatory T Cells (Tregs)

In order to achieve the desired clinical outcome (complete tumor cell eradication), the immune response must continue until all tumor cells have been eradicated. However, complete eradication also needs to be followed by a cessation of the adaptive immune response to prevent autoimmune disease [4]. In general, regulatory T cells help bring the immune response to an eventual end in several important ways. Regulatory T cells can kill

antigen presenting dendritic cells, and alter dendritic cell function to become toxic towards CTLs [42]. Tregs can also hinder the activation and migration of dendritic cells [51]. Tregs are also capable of directly killing active CTLs or decreasing proliferation rates of active CTLs [42, 4]. This type of suppressive activity actually prevents an organism’s own immune system from attacking healthy cells once the threat is over [4]. Unfortunately, this means that Tregs aid cancerous tumors to actually keep CTLs from killing tumor cells [51, 43]. One of the primary focuses of cancer immunotherapy is adequately suppressing Tregs to allow for an immune response sufficient to eradicate all tumor cells while not overly suppressing Tregs, which can cause autoimmune disease [52, 51, 43, 44].

1.7 B Cells and Antibodies

B cells congregate in the lymph nodes until antigen has been presented and eventual activation occurs [4]. However, in many cases these cells still require an additional stimulus from activated helper T cells to be activated [4]. After antigen presentation and a secondary stimulus via activated helper T cells has occurred, B cells become fully activated plasma B cells that can produce antibodies specific to the laser irradiated tumor cells [12, 53, 4]. These antibodies then move to the site of tumors and “tag” them for destruction by innate immune cells like natural killer cells (NKs) or macrophages [12, 53, 4, 54]. Activated B cells can also activate naive helper T cells [4].

1.8 Immunoadjuvants and Elements of Treatment

Immune adjuvants affect different components of the immune system in a variety of ways. Ultimately, their purpose is to make the immune response more efficient [55]. Adjuvants are used with vaccines in order to help facilitate antigen uptake and processing via antigen presenting cells like dendritic cells [55]. They can also increase dendritic cell migration rates and make antigen presentation to cytotoxic T cells more efficient [55]. In anti-tumor laser immunotherapy, the immune adjuvant GC is injected intratumorally either before or after laser treatment [11, 12, 13, 14, 15, 16, 17, 18]. It is not entirely known exactly how GC affects the immune system, but one observed outcome is that macrophages and natural killer cells become more active at tumor sites as GC concentration increases [56]. However, its administration has been shown to lead to a more robust adaptive immune response similar to that of other adjuvants [12, 15, 18, 56]. Therefore, we analyze the effects of GC based on the assumption that this substance behaves similarly to other immune adjuvants.

CHAPTER 2

MATHEMATICAL MODEL

We have written and analyzed a model that includes only DCs, CTLs, tumor cells, and tumor antigen (see appendix for related models). However, we are able to implicitly study the effects of Tregs, helper T cells, B cells, and antibodies by varying parameters in our model. This allows us to analyze a model that is roughly half the size of the full system and has far fewer parameters (compare the model in Equations 2.1 to the similar, but expanded, model in Equations A.1). Based on work presented in [11, 12, 13, 14, 15, 16, 17, 18], we identify a subset of host immune cells activated during tumor immunotherapy that contribute to tumor eradication (see Figure 2.1). We propose that these cells and their interactions are the mechanism that underlies tumor clearance via laser immunotherapy (LIT).

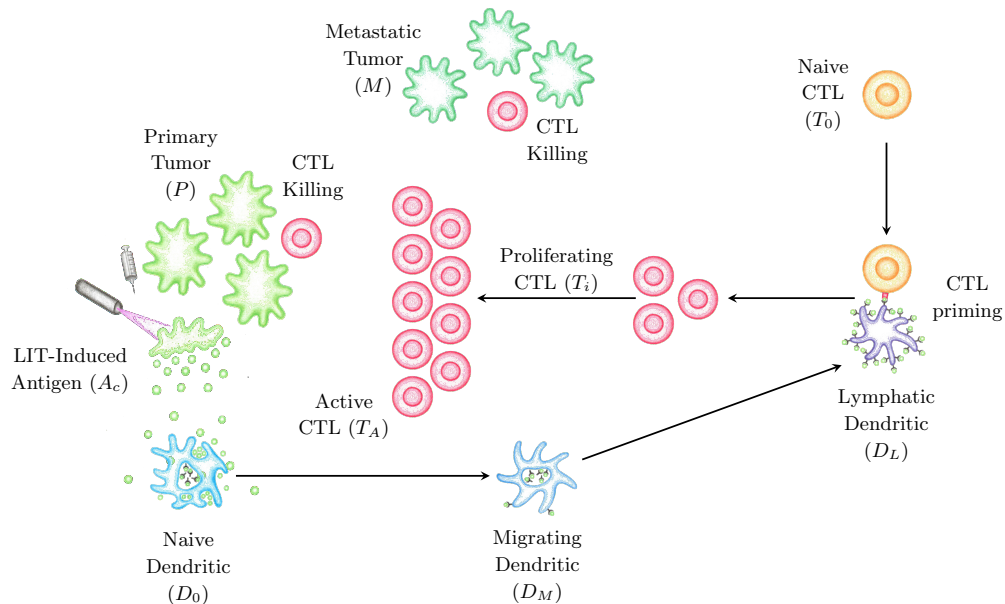


Figure 2.1. Conceptual model of antitumor laser immunotherapy. After LIT, antigen (A_c) is released. Naive dendritic cells (D_0) take up antigen, begin migrating (D_M), and reach lymph nodes (D_L) to present antigen to naive CTLs (T_0). CTLs enter stages of proliferation ($T_1 - T_n$). After proliferation, CTLs (T_A) kill primary (P) and metastatic (M) tumors.

2.1 Mathematical Model

The model is a system of first-order, nonlinear, ordinary differential equations that are nearly autonomous, with the exception of a forcing function. The function $\phi(t)$ is a unitless time-dependent treatment function responsible for primary tumor cell death driven by the laser-tissue interaction. In Equations 2.1, we track each stage of maturation of DCs and CTLs, the tumor antigen load, and the primary and metastatic tumor burdens.

$$\begin{aligned}
\left(\begin{array}{c} \text{Naive} \\ \text{Dendritic} \end{array} \right) & \frac{dD_0}{dt} = s_d - (\alpha A_c + \delta_{D_0}) D_0 \\
\left(\begin{array}{c} \text{Migratory} \\ \text{Dendritic} \end{array} \right) & \frac{dD_M}{dt} = \varepsilon_M \alpha A_c D_0 - (\eta + \delta_{D_M}) D_M \\
\left(\begin{array}{c} \text{Lymphatic} \\ \text{Dendritic} \end{array} \right) & \frac{dD_L}{dt} = \varepsilon_L \eta D_M - \delta_{D_L} D_L \\
\left(\begin{array}{c} \text{Naive} \\ \text{CTL} \end{array} \right) & \frac{dT_0}{dt} = s_t - (\beta D_L + \delta_{T_0}) T_0 \\
\left(\begin{array}{c} 1^{\text{st}} \text{ stage} \\ \text{CTL} \end{array} \right) & \frac{dT_1}{dt} = \varepsilon_1 \beta D_L T_0 - (\xi T_1 + \delta_{T_0}) T_1 \\
\left(\begin{array}{c} i^{\text{th}} \text{ stage} \\ \text{CTL} \end{array} \right) & \frac{dT_i}{dt} = \varepsilon_i \xi T_{i-1} - (\xi T_i + \delta_{T_0}) T_i, \quad \text{for } i = 2, \dots, n \\
\left(\begin{array}{c} \text{Active} \\ \text{CTL} \end{array} \right) & \frac{dT_A}{dt} = \varepsilon_A \xi T_n - k \delta_{T_0} T_A \\
\left(\begin{array}{c} \text{Primary} \\ \text{Tumor} \end{array} \right) & \frac{dP}{dt} = \gamma_P P - \left(\mu + \phi(t) + \frac{\lambda_P T_A}{c_p + T_A} \right) P \\
\left(\begin{array}{c} \text{Metastatic} \\ \text{Tumor} \end{array} \right) & \frac{dM}{dt} = \sigma \mu P + \gamma_M M - \left(\frac{\lambda_M T_A}{c_m + T_A} \right) M \\
\left(\begin{array}{c} \text{Tumor} \\ \text{Antigen} \end{array} \right) & \frac{dA_c}{dt} = \rho \phi(t) P + p \left(\frac{\lambda_P T_A P}{c_p + T_A} + \frac{\lambda_M T_A M}{c_m + T_A} \right) - (\omega + \varepsilon_{A_c} \alpha D_0) A_c
\end{aligned} \tag{2.1}$$

Sample results of the model given in Equations 2.1 are illustrated in Figure 2.2 and Figure 2.3, which are explained in greater detail in the subsequent section (see Chapter 3, specifically Section 3.2). Model parameters and units are shown in Table 2.2.

Each of the equations governing immune dynamics is derived similarly based on the underlying biological dynamics. Initially, there is a naive (inactive) population of cells that eventually gives rise to intermediate and active populations. Both DCs and CTLs go through intermediate developmental phases before complete activation occurs. Each immune population naturally decays due to mortality at some natural rate, δ_{D_i} for DCs and δ_{T_0} for CTLs. Naive dendritic cells (D_0) are produced at a constant rate s_d . Naive dendritic cells interact with tumor antigen (A_c) at a mass action rate α which drives a transition into the migratory dendritic cell state (D_M) with efficiency ε_M . Migration occurs at rate η , as migrating dendritic cells move to the lymph nodes. Upon some fraction (ε_L) reaching a lymph node, we consider dendritic cells to be fully activated lymphatic dendritic cells (D_L).

Similarly for CTL equations, there is a constant supply rate s_t into the naive population (T_0). Once lymphatic DCs present antigen to naive CTLs at rate β , stimulated T cells enter

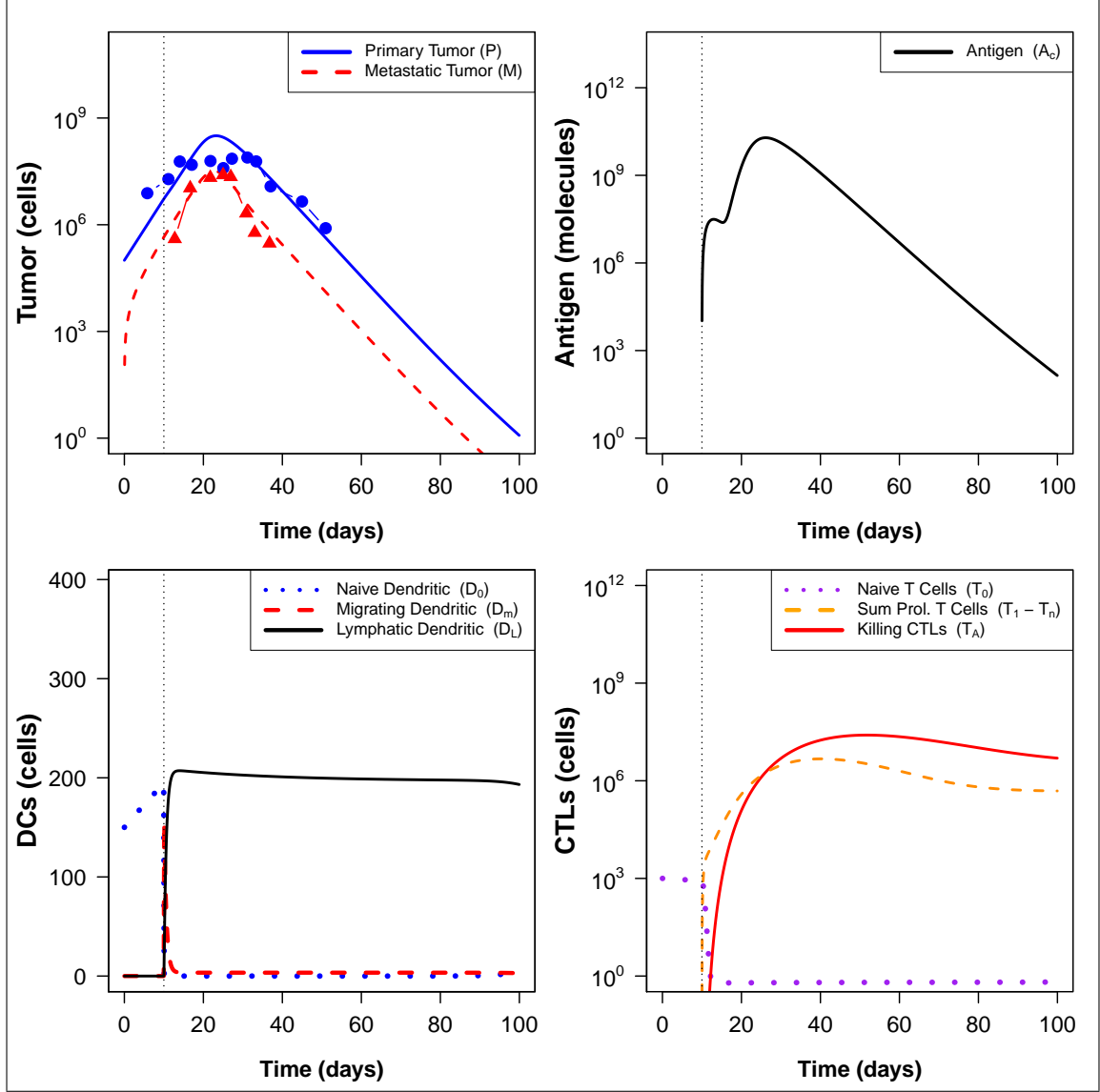


Figure 2.2. Predicted tumor-immune dynamics demonstrating the general case of successful treatment. Primary and metastatic tumor burden data from [15]. In the upper left plot, solid blue dots are primary tumor burden experimental data and solid red triangles are metastatic tumor burden experimental data. Solid, dashed, and dotted curves in each plot are model simulations. Vertical dashed line in each plot represents the time of laser treatment at $t = 10$ days. In the lower right plot, CTL dynamics are shown for $n = 8$ proliferative stages. The orange dashed curve in the lower right plot is the total number of proliferating CTLs (i.e. $\sum_{i=1}^n T_i(t)$).

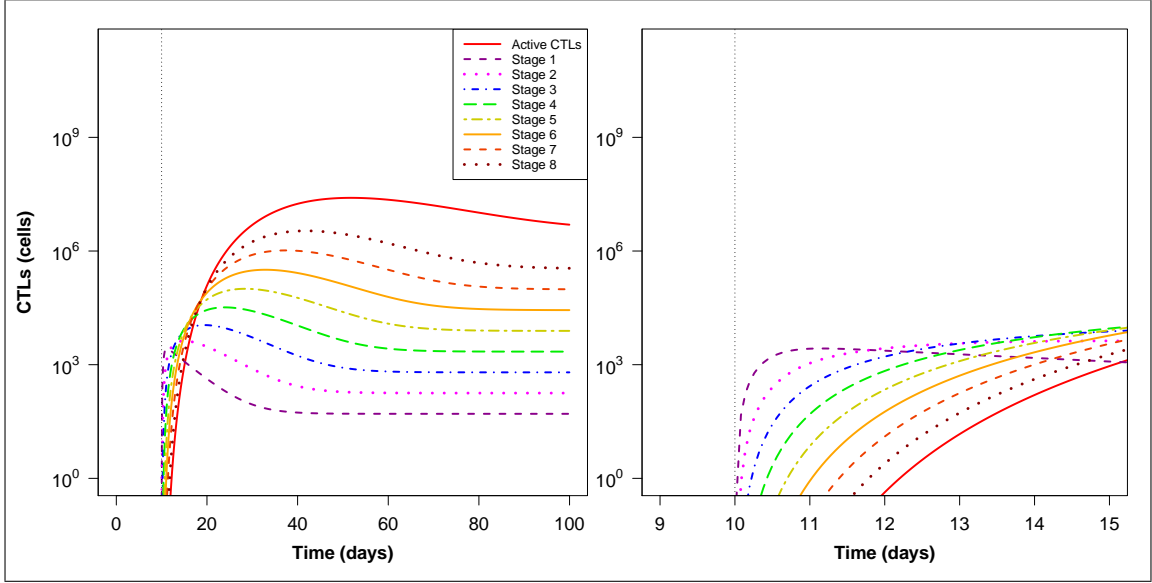


Figure 2.3. (Left) Progression through the stages of proliferation with the highest curve ($t \geq 40$) being the active CTLs able to kill tumor cells. For $t \geq 40$, the lowest curve represents the first proliferative stage. Each successively higher curve represents the i^{th} proliferative stage for $i = 2, 3, \dots, 8$. (Right) The same CTL proliferative stages on a smaller scale $t \in [9, 15]$.

several stages of proliferation ($T_1 - T_n$) where we chose $n = 8$ based on proliferation data in the literature [57]. During the proliferative stages, each cell will clone itself, expanding its lineage by a factor ε_i . This expansion gives rise to the i^{th} -stage equation in the model. Proliferative T cells move from one stage to the next at rate ξ . After the n^{th} stage, CTLs have fully proliferated and become completely activated (T_A) and begin killing tumor cells. Though not modeled, CTLs can be re-stimulated by other immune cells so that they live for extended periods in the active state, but these cells generally die more quickly [4]. Thus, we introduce a scaling factor k to account for increased CTL death.

With initial conditions at 10^5 cells, the primary tumor cells (P) grow exponentially at rate γ_p . We assume that primary tumor cells metastasize exponentially at some rate μ giving rise to metastatic tumor cells (M) with efficiency σ . We do not address multiple metastatic tumors explicitly, but instead track the aggregate population. The population of metastatic tumor cells in our model is the total amount of cells that have left the primary tumor and continue to expand. Once tumor cells become metastatic, they continue to grow exponentially at rate γ_M . Killing of tumor cells is assumed to be proportional to the

effectivity of CTL killing $\frac{T_A}{c_i+T_A}$. Ultimately, the per capita killing rate λ_i and the constant c_i determines the effectiveness of killing.

Tumor antigen is partly created by laser irradiation of the primary tumor, which is modeled by a time-dependent function $\phi(t)$. This function is equal to zero until time of treatment at $t = 10$ days. It is defined as 0 for $0 \leq t < 10$ and as $0.1(t - 10)e^{-(t-10)}$ for $t \geq 10$. Antigen is also created when CTLs kill primary and metastatic tumor cells which is shown by the addition of terms $\frac{\lambda_p T_A P}{c_p + T_A}$ and $\frac{\lambda_m T_A M}{c_m + T_A}$ in the (A_c) equation. Antigen is naturally cleared at rate ω and is taken up by naive DCs at rate α with efficiency ε_{A_c} . Tumor killing will continue, whether it is effective or not, until all antigen has been cleared.

2.2 Parameterization

Since patients have innate immune parameters in the absence of tumors, we have a group of parameters associated to the patient himself (e.g. constant supplies for naive populations s_t and s_d). Still other parameters may be more closely associated to the tumors, such as growth (γ_p and γ_M) and antigenicity (ρ and σ), so we separate these parameters from the rest. In planning and analyzing numerical experiments with Treg and GC effectivity, we are able to partition parameters according to each category of influence. These relationships are illustrated in Figure 2.4, which shows all of the treatment parameters organized into essentially non-overlapping groups within the patient. A detailed list for each categorical parameter is given in Table 2.2.

The patient encompasses all cellular and molecular components, so this can be defined as the universal set of the diagram. Subsets for Treg and GC parameters intersect because both have influence on the DC migration rate η . Similarly, GC and cancer parameters intersect since both affect the rate of metastasis μ . Specific numerical values and ranges are quoted in Table 2.2.

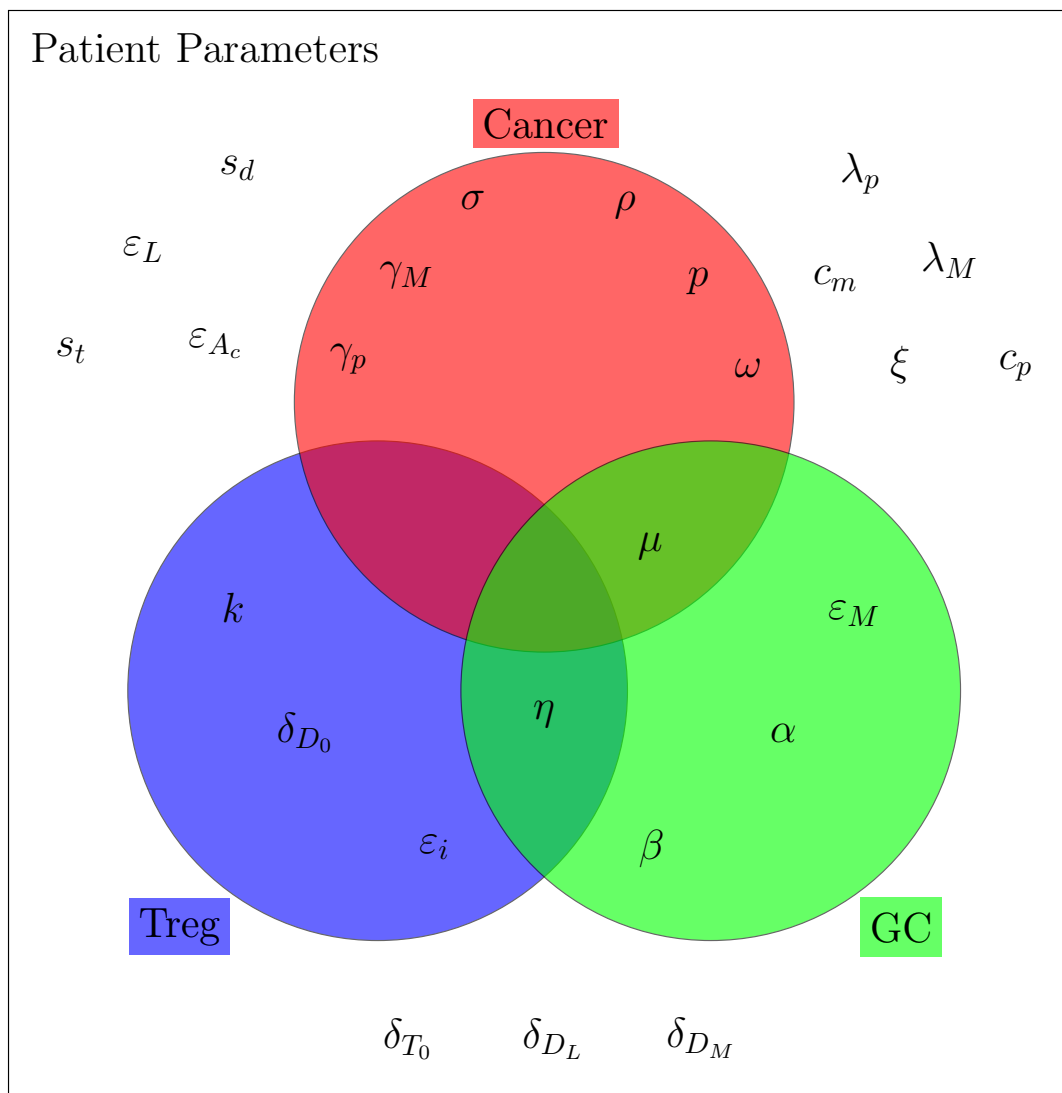


Figure 2.4. Parameters categorized by innate patient associated parameters, cancer associated parameters, Treg associated parameters, and GC associated parameters. The patient parameter set includes all parameter subsets. The parameter ϵ_i is indexed by $i = 1, 2, \dots, 8$ for proliferating cells and A for fully-activated cells.

Table 2.1. Symbols, values, units, and references for patient parameters used in the system given in Equations 2.1. These parameters are those that are innate to the patient in the absence of cancer. Parameters without references were estimated by minimizing the root mean squared error (RMSE) with LHS from data in [15].

Parameter	Value	Units	Reference
Patient			
s_t	3.3	$\frac{T_0 \text{ cells}}{\text{day}}$	estimated
s_d	5	$\frac{D_0 \text{ cells}}{\text{day}}$	estimated
ε_L	0.95	$\frac{D_L \text{ cells}}{D_M \text{ cells}}$	estimated
λ_P	0.925	$\frac{1}{\text{day}}$	estimated
λ_M	0.875	$\frac{1}{\text{day}}$	estimated
δ_{D_M}	0.027027027	$\frac{1}{\text{day}}$	[58]
δ_{D_L}	0.1111111111	$\frac{1}{\text{day}}$	[4]
δ_{T_0}	0.0187337076	$\frac{1}{\text{day}}$	[59]
c_p	10^5	T_A cells	estimated
c_m	10^4	T_A cells	estimated
ξ	0.25	$\frac{1}{\text{day}}$	estimated
ε_{A_c}	1	$\frac{A_c \text{ molecules}}{D_0 \text{ cells}}$	estimated

Table 2.2. Symbols, values, units, and references for regulatory T cell, cancer, and glycated chitosan parameters used in the system given in Equations 2.1. Treg dynamics, cancer dynamics, and GC dynamics. Parameters without references were estimated by minimizing the root mean squared error (RMSE) with LHS from data in [15].

Parameter	Value	Units	Reference
Cancer			
γ_P	0.63	$\frac{1}{\text{day}}$	estimated
γ_M	0.2	$\frac{1}{\text{day}}$	estimated
μ	0.008	$\frac{1}{\text{day}}$	estimated
σ	0.45	$\frac{M \text{ cells}}{P \text{ cell}}$	estimated
ρ	100	$\frac{A_c \text{ molecules}}{P \text{ cell} \cdot \text{day}}$	estimated
p	1	$\frac{A_c \text{ molecules}}{\text{tumor cell}}$	estimated
ω	1	$\frac{1}{\text{day}}$	estimated
Treg			
k	4.163995	unitless	none
δ_{D_0}	0.027027027	$\frac{1}{\text{day}}$	[58]
ε_A	3	$\frac{T_A \text{ cells}}{T_n \text{ cell}}$	[60]
ε_i	3	$\frac{T_i \text{ cells}}{T_{i-1} \text{ cell}}$	[60]
η	0.9	$\frac{1}{\text{day}}$	[4]
Glycated Chitosan			
α	0.012	$\frac{1}{\text{Molecule} \cdot \text{day}}$	estimated
β	0.0183622094883075	$\frac{1}{D_L \text{ cell} \cdot \text{day}}$	estimated
ε_M	0.95	$\frac{D_M \text{ cells}}{D_0 \text{ cell}}$	estimated
η	0.9	$\frac{1}{\text{day}}$	[4]
μ	0.008	$\frac{1}{\text{day}}$	estimated

CHAPTER 3

ANALYSIS OF MATHEMATICAL MODEL

In order to understand the intricate details of anti-tumor laser immunotherapy as described in [11, 12, 13, 14, 15, 16, 17, 18, 56], the following questions must be answered.

1. What is the baseline growth pattern for the DMBA-4 metastatic mammary tumor cell line used in animal model studies for anti-tumor laser immunotherapy?
2. To link mathematical modeling results to animal model experimental data, can we classify model dynamics and relate results to animal model data?
 - (a) What are the qualitative and quantitative properties of what would be considered successful or failed treatment?
 - (b) In performing sensitivity analysis with parameters, what does the model predict about the diversity of treatment outcomes?
 - (c) What features of anti-tumor laser immunotherapy can be modified and what impact would these changes have on treatment outcome or post-treatment dynamics?
3. What is the role of GC in the development and dynamics of the immune response?
 - (a) How does GC affect tumor-immune dynamics after laser treatment, and how can these effects be captured by and studied with a mathematical model?
 - (b) What model parameters could be changed to study the effects of varying levels of glycosylated chitosan effectivity?
4. The importance of Treg suppression on immunotherapy outcome has been demonstrated experimentally. Which modeled components are influenced by Treg regulation and would benefit from Treg suppression?
 - (a) Since the model does not explicitly include Tregs, how can their effects be modeled implicitly by changing key parameters that correspond to levels of Treg immunosuppressive activity?
 - (b) Can the model be used to link a patient's clinical outcome with a given level of Treg immunosuppressive activity?

3.1 Sensitivity Analysis

In order to more comprehensively explore the post-treatment dynamics that the model predicts, it is necessary to solve the model for a considerably large number of different parameter sets. It is desirable to minimize the number of parameter sets that must be sampled to develop an overall concept of the model's behavior. We also sample parameters within a pre-defined range to adhere to as many biologically known parameters as possible. To accomplish these goals, a method called Latin Hypercube Sampling (LHS) is used to randomly generate 1000 different parameter sets [61].

3.1.1 Latin Hypercube Sampling

For LHS, each parameter is considered a random variable with some probability distribution function [62, 61]. Each parameter distribution is then divided into n intervals of equal probability from which values are selected without replacement [62, 61] (see Figure 3.1). Thus, if there are k parameters and one desires to sample n values for each parameter from its distribution, then the final result will be an $n \times k$ matrix of n generated values for each of the k parameters.

The LHS method provides efficient approximation of each probability distribution function due to the fact that it allows only a single value to be randomly selected in any one interval of the n -interval subdivision of the parameter probability distribution function [62, 61]. The random nature of this selection technique also ensures that a large portion of the parameter space is sampled [62]. LHS is superior to simple random sampling of parameters, with the assumption of some probability distribution function for a given parameter, due to more efficient and broad exploration of each parameter space [62, 61]

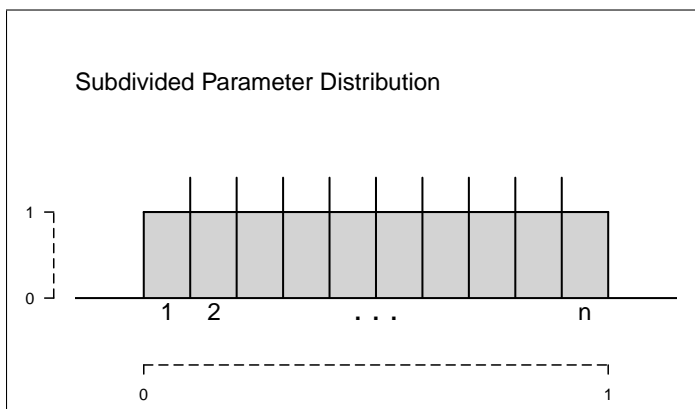


Figure 3.1. Example of how the uniform distribution for each parameter is divided into equally probable intervals from which sampling will take place without replacement. Sampling the uniform distribution with equally probable intervals implies that the intervals are all of the same length. Assuming a different distribution would lead to unequal intervals to ensure equally probable selection.

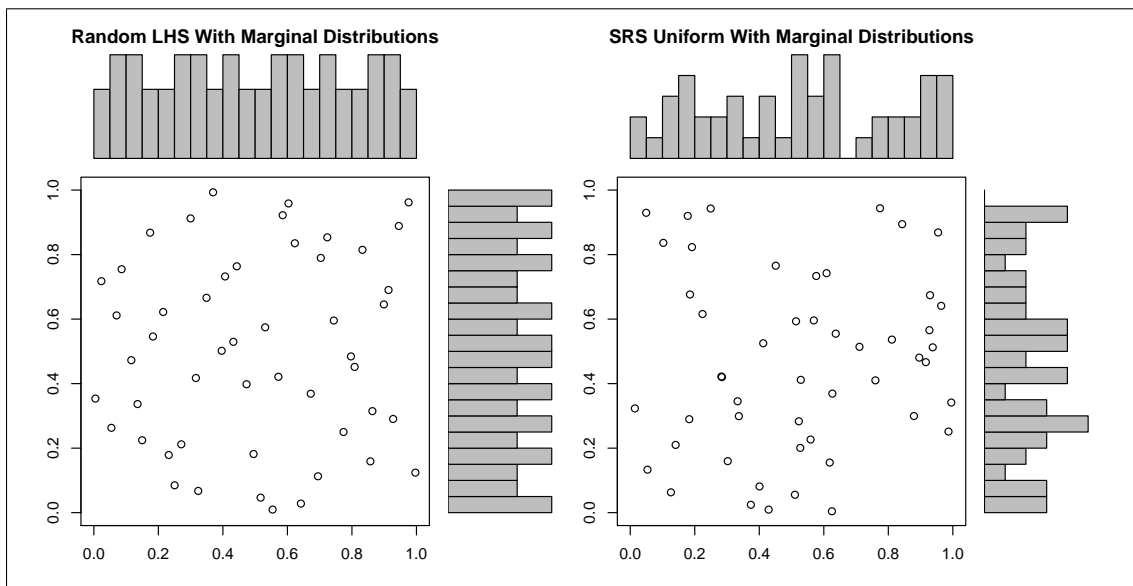


Figure 3.2. Scatterplot of 50 points in the unit plane sampled with (on left) random LHS and (on right) simple random sampling (SRS) of the uniform distribution on $[0,1]$. Marginal distribution histograms above and to the right scatterplot show the efficiency of random LHS and SRS in estimating the uniform distribution on $[0,1]$. Based on this comparison between LHS and SRS, it is clear that LHS is a better approximation of the uniform distribution for the 50 points.

(see Figure 3.2).

Implementation of the Latin Hypercube design for sampling model parameters was done using the `randomLHS(n, k)` function in the *R* [63] ‘lhs’ package [64], where n is the number of generated parameter sets and k is the number of parameters. With the `randomLHS()` function, values for each parameter are selected randomly from the uniform distribution on $[0, 1]$. We constrained parameter values since biological rates are not arbitrary, so we are able to define a minimum ($pMin$) and a maximum ($pMax$) for each parameter. We choose $pMin$ and $pMax$ to be a scaled multiple of the baseline parameter value. In the context of analyzing model sensitivity to changes in parameter values, the assumption of a uniform distribution for each parameter could be replaced by another distribution. However, the qualitative outcomes of model simulation will be the same regardless of the distribution since sampled parameters will be scaled to be between $pMin$ and $pMax$.

Once all n sets of parameters have been randomly selected, the result is an $n \times k$ matrix (Latin Hypercube) where the ij^{th} entry is the i^{th} selection of the j^{th} parameter. After the $n \times k$ matrix is generated, parameters must be scaled so that they remain confined to our pre-defined range. Transformation is calculated by

$$pGen = pGen(pMax - pMin) + pMin$$

where $pGen$ is one of the generated parameter values in the $n \times k$ matrix with corresponding maximum and minimum values $pMax$ and $pMin$. Since the parameter distribution is defined to be uniform on $[0, 1]$, the maximum value that $pGen$ can have is 1. If this is the case, then the above formula reduces to

$$pGen = pMax$$

where $pGen$ is the given maximal value within its pre-defined range. Similarly, the minimum value $pGen$ can have is 0. If this is the case, then the rescaling formula becomes

$$pGen = pMin$$

where $pGen$ is the given minimal value within its pre-defined range. After all entries in the $n \times k$ matrix have been rescaled, the result is a new $n \times k$ matrix with n randomly generated values for all k parameters such that each value is within its allowable range $[pMin, pMax]$.

3.2 Predictions of Treatment Outcomes

Treatments are typically performed 10 - 15 days after approximately 10^5 viable DMBA-4 metastatic mammary tumor cells are injected into each rat [12, 13, 14, 15, 16, 17, 18]. Tumors are injected with a solution composed of a photosensitizing agent called indocyanine green and the immunoadjuvant glycated chitosan, and then irradiated for about 10 minutes [12, 13, 14, 15, 16, 17, 18]. Post-treatment, the primary tumor continues to grow until it reaches a peak in a range of 30 - 50 days following treatment [12, 13, 14, 15, 16, 17, 18]. Once a global peak has been reached for primary tumor burden, tumors begin to shrink in size to eventual depletion within 100 days after treatment [12, 13, 14, 15, 16, 17, 18]. Since tumor burden of treated rats in these experiments exhibits exponential growth and decay, the mathematical model takes this into account using the simple exponential population growth model.

The model produces the general case of successful treatment outlined above with data from [15]. The model simulation of the general treatment dynamics for tumor burden shown in [12, 13, 14, 15, 16, 17, 18], as well as the associated immune system dynamics predicted by the model is shown in Figure 3.3. Model solutions were found using `lsoda()` function in the *R* ‘deSolve’ package [65]. Using LHS of patient parameters, 1000 parameter sets were generated. The model was solved for each parameter set, and the solution that

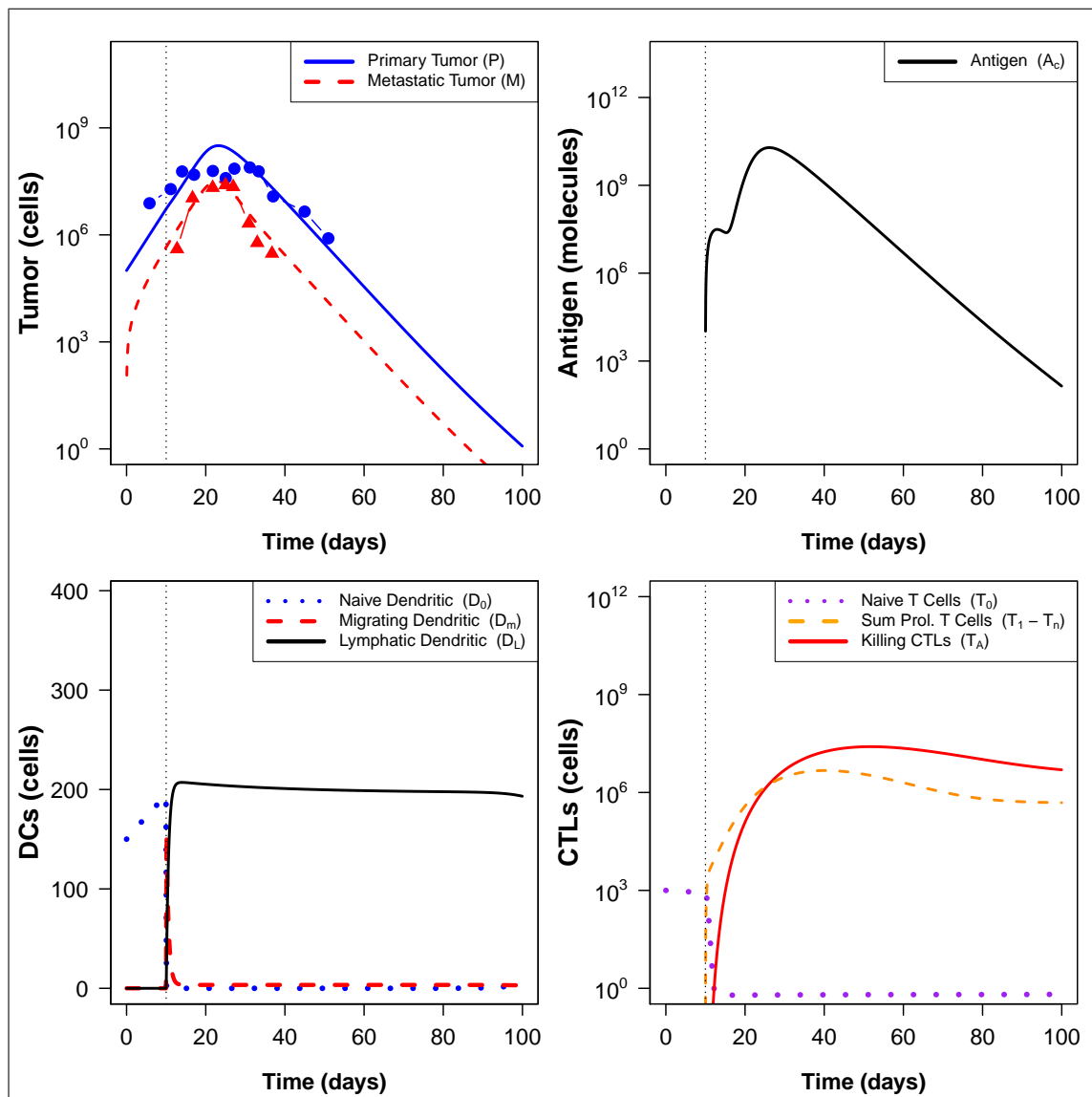


Figure 3.3. Reproduced from Figure 2.2 in Section 2.1. Predicted tumor-immune dynamics demonstrating the general case of successful treatment. Primary and metastatic tumor burden data from [15]. In the upper left plot, closed black dots are primary tumor burden experimental data and open triangles are metastatic tumor burden experimental data. Solid and dashed curves in each plot are model simulations. Vertical dashed line in each plot represents the time of laser treatment at $t = 10$ days. In the lower right plot, CTL dynamics are shown for $n = 8$ proliferative stages. The orange curve in the lower right plot is the total number of proliferating CTLs (i.e. $\sum_{i=1}^n T_i(t)$).

minimized the root mean squared error was chosen to produce Figure 3.3. The data chosen for comparison is in [15]. The upper left-hand plot in Figure 3.3 shows model simulation for primary and metastatic tumor burdens with tumor burden data for each tumor type. The tumor burden simulation reflects experimental observations since the tumor burden curves increase to a peak between days 20 and 40, and then gradually decay to zero by the end of the simulated period. This figure also shows the dynamics of tumor antigens. The model simulation shows that there is an abrupt increase due to laser treatment and CTL-mediated tumor cell killing. Antigen is slowly cleared as the tumor burden curves decay to zero.

In the lower left plot of Figure 3.3, dendritic cell dynamics are shown. The simulation shows an initially existing population of naive dendritic cells that quickly decays due to laser treatment at $t = 10$ days. These naive cells quickly become migratory cells, which then become lymphatic dendritic cells. The solid black curve in the dendritic cell plot represents the number of lymphatic dendritic cells. Since the tumor burden curves gradually decay until the end of the treatment simulation, the lymphatic dendritic cell curve does not significantly deviate from its maximum.

The lower right plot of Figure 3.3 shows model simulation for CTL dynamics. The simulation shows an initially existing population of naive CTLs that quickly decays due to lymphatic dendritic cell interaction. The solid red curve represents the total number of actively killing CTLs after all of the proliferative stages have been completed. This simulation shows the slight delay between CTL activation and the introduction of CTLs to the tumor sites. Simulated curves for actively killing CTLs quickly increase to a maximum between days 40 and 50, and then gradually decay until the end of the simulated period.

Model simulation of each proliferative CTL stage and the actively killing CTLs is shown in Figure 3.4. The lowest curve ($t \geq 40$) in this plot represents the first proliferative stage. Each successively higher curve represents the i^{th} proliferative stage (for $i = 2, 3, \dots, 8$). The solid red curve represents the actively killing CTL population. This simulation comes from the same solution as shown in Figure 3.3, where proliferative stages were summed to draw focus on the active CTL stage.

In experimentally treated animals, there are several types of qualitative treatment outcomes ranging from tumor clearance resulting in patient survival to tumor escape resulting in the death of the patient [11, 12, 13, 14, 15, 16, 17, 18]. Based on the results of animal experiments [11, 12, 13, 14, 15, 16, 17, 18], one of the following clinical outcomes is assigned to each model simulation (see Figure 3.5):

Clearance - tumors are controlled quickly, primary tumor burden does not exceed 3×10^{10} cells, and primary tumor burden is below 10^0 cell by the end of the simulated study period (solid green curves)

Slow Clearance - primary tumor burden clears slowly but not completely, there has not been a relapse, and primary tumor burden does not exceed 3×10^{10} cells (dashed blue curves)

Relapse - initial clearing of primary tumor burden with eventual re-growth to an obvious peak, and primary tumor burden does not exceed 3×10^{10} cells (dotted purple curves)

Death - primary tumor burden exceeds 3×10^{10} cells and study animal is sacrificed (dashed and dotted red curves)

It is known that different organisms within the same species routinely exhibit vastly different immunities [4]. For the mathematical model, these immunological variances are expressed by changes to model parameters. In line with the concept of random immune variability, 1000 different parameter sets were randomly generated by LHS. For each parameter set, the model was solved with fixed initial conditions.

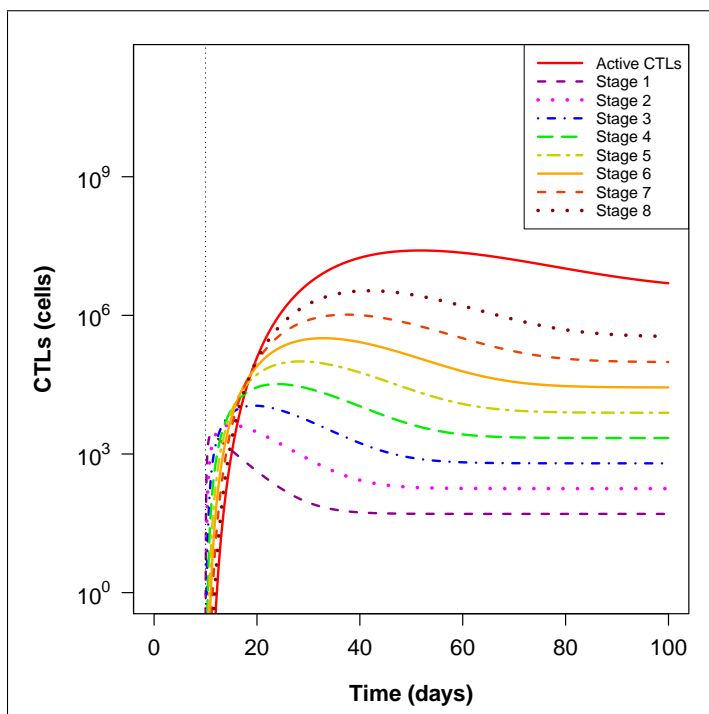


Figure 3.4. Reproduced from Figure 2.3 in Section 2.1. Progression through the stages of proliferation with the highest curve ($t \geq 40$) being the active CTLs able to kill tumor cells. For $t \geq 40$, the lowest curve represents the first proliferative stage. Each successively higher curve represents the i^{th} proliferative stage for $i = 2, 3, \dots, 8$.

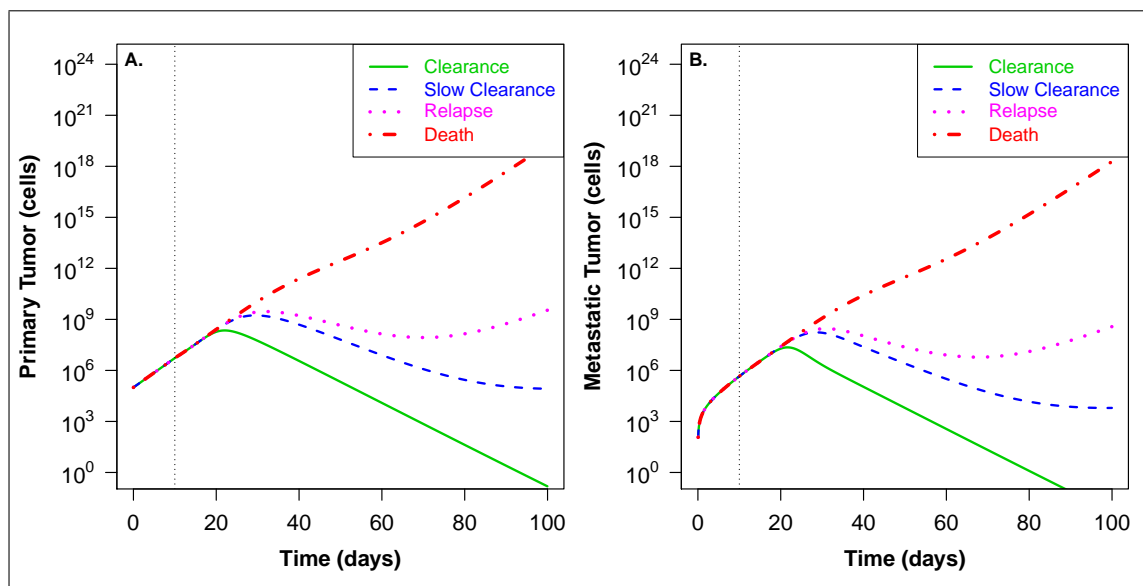


Figure 3.5. Model simulations produced as patient parameters vary about baseline parameter set using LHS. All qualitatively different outcomes, as defined previously (Section 3.2), are represented. (A) Changes in primary tumor burden as patient parameters vary. (B) Changes in metastatic tumor burden as patient parameters vary.

3.3 Modeling the Effects of Glycated Chitosan (GC)

Immunoadjuvants are used to stimulate the immune system to achieve a more robust immune response [66, 55]. In [11, 12, 13, 14, 15, 16, 17, 18, 56], the immunoadjuvant glycated chitosan is used to stimulate the immune system in antitumor laser immunotherapy. Immunoadjuvants have been shown to increase antigen uptake, aid in dendritic cell activation and maturation/migration, and aid in T cell activation [66, 55]. With the reasonable assumption that glycated chitosan adopts a similar mode of immune stimulation, we can model these effects by changing corresponding model parameters. Parameters that change with varying levels of GC effectivity are:

- α - rate at which dendritic cells interact with antigen and become activated
- η - rate of dendritic cell migration
- ε_M - efficiency of naive to migratory dendritic cell conversion
- β - rate at which lymphatic dendritic cells interact with and activate naive CTLs
- μ - rate of primary tumor cell metastasis

Using LHS of GC parameters, 1000 different GC parameter sets were randomly generated. For each parameter set, the model was solved with fixed initial conditions to determine

model sensitivity to changes in GC levels. Simulations were qualitatively classified by changes in overall tumor dynamics as outlined previously in Section 3.2.

Model sensitivity to changes in GC parameters is demonstrated in Figure 3.6. The first column of this figure represents tumor burden dynamics for each outcome. The most noticeable change from the effects of GC is shown in the second column, which represents dendritic cell dynamics for varying degrees of GC effectivity. In the last row, the extremely low number of DCs in the lymph nodes affects the eventual number of activated CTLs. This in turn produces a tumor burden that is uncontrolled, which corresponds to patient death.

A comparison of each clinical outcome on the same plot for selected cell types is given by Figure 3.7. Figure 3.7(A), showing primary tumor burden dynamics, illustrates how changes in GC parameters can alter clinical outcome from clearance (solid green curve) to death (dotted red curve). Results are similar in Figure 3.7(B), but with metastatic tumor burden instead. Figure 3.7(C-D) may seem somewhat contradictory since there are more lymphatic dendritic cells and CTLs in the slow clearance case. However, from Table 3.1, the rate of metastasis is larger in the clearance case when compared to the slow clearance case. This leads to greater decline in primary tumor burden since tumor cells are both metastasizing and being killed by CTLs simultaneously.

Table 3.1. Changes in GC parameters from one clinical treatment outcome to the next. η is the DC migration rate to lymph nodes, β is the lymphatic DC - CTL interaction rate, ε_m is the naive to migratory DC efficiency, μ is the rate of metastasis, and α is the interaction rate between naive DC and free antigen.

Outcome	η	β	ε_M	μ	α
Clearance	1.003541	0.0001248971	0.6624288	0.1869302	8.190×10^{-5}
Slow Clearance	0.9220876	3.157×10^{-5}	0.8573427	0.05970596	1.267×10^{-5}
Dead	1.391807	4.086×10^{-5}	0.04326611	0.03730337	7.844×10^{-5}

changes in GC parameters can alter clinical outcome from clearance (solid green curve) to death (dotted red curve). Results are similar in Figure 3.7(B), but with metastatic tumor burden instead. Figure 3.7(C-D) may seem somewhat contradictory since there are more

lymphatic dendritic cells and CTLs in the slow clearance case. However, from Table 3.1, the rate of metastasis is larger in the clearance case when compared to the slow clearance case. This leads to greater decline in primary tumor burden since tumor cells are both metastasizing and being killed by CTLs simultaneously.

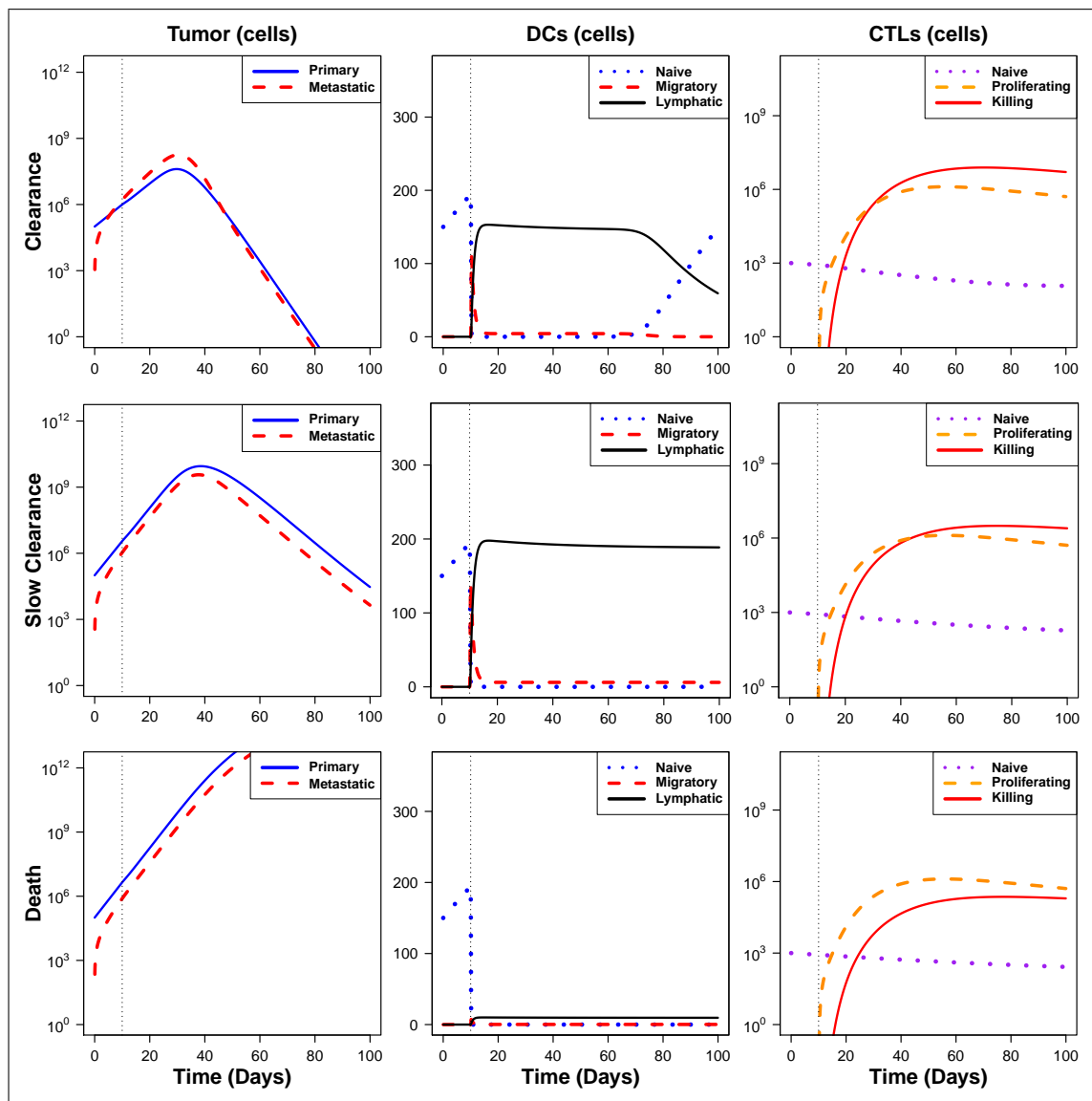


Figure 3.6. For each clinical outcome (corresponding to rows) defined by tumor dynamics, simulations for each cell type are shown. Clinical outcome is highly correlated with the maintenance of CTLs throughout the simulated treatment. This indirectly indicates that clinical outcome becomes more favorable as GC effectivity increases. Variation in GC parameters did not produce clinical outcome of tumor relapse.

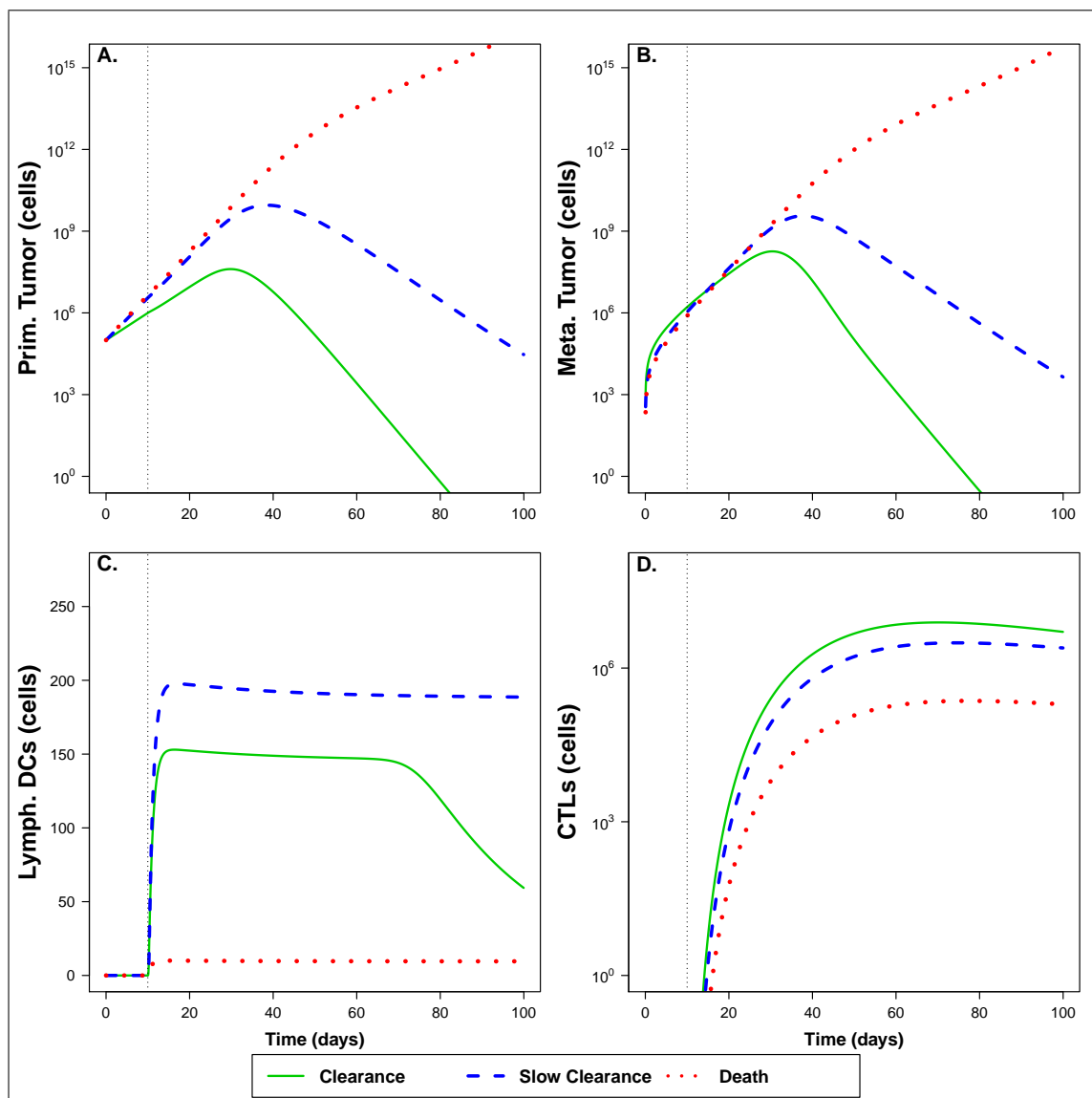


Figure 3.7. Depiction of changes in cellular dynamics as GC effectivity changes. In each panel, the clinical outcome of clearance (i.e., patient survival) is in solid green, the clinical outcome of slow clearance (prolonged survival) is in dashed blue curve, and the clinical outcome of death is in dotted red. Variation in GC parameters did not produce clinical outcome of tumor relapse.

3.4 Regulatory T Cell Experimental Simulation

Based on the immunosuppressive activity of regulatory T cells outlined in Section 1.6.3, Treg effects can be modeled by their influence on corresponding model parameters. Param-

eters that change with varying levels of Treg activity are:

- δ_{D_0} - naive dendritic cell death rate (changes due to Tregs killing DCs)
- ε_A - proliferation constant for CTLs (changes due to Treg interference)
- k - death scaling constant for active CTLs (changes due to Tregs killing CTLs)
- η - migration rate for dendritic cells to lymph nodes (changes due to Treg interference).

Using LHS of Treg parameters, we randomly sampled 1000 different parameter sets from each Treg parameter's uniform distribution. Sampled parameters were then scaled to a conservative range about each predefined baseline parameter value. The model was solved for each parameter set with fixed initial conditions to produce results shown in Figures 3.8 and 3.9, which are classified according to overall tumor burden dynamics outlined previously in Section 3.2.

The motivation for using LHS of Treg parameters primarily comes from the desire to efficiently explore the Treg parameter space. The interpretation of the hypercube matrix output is that each row corresponds to a unique level of Treg effectivity. The uniqueness comes from the fact that each row contains no identical entries to any other row. This is highly representative of the random variability in each individual's immune parameters. However, since we desire to search a Treg parameter space with a much larger range than would generally be attributed to natural individual variation, we may also interpret each row of the hypercube matrix to represent the effects of various immunosuppressive drugs on Treg activity.

We interpreted the hypercube generated with Treg parameters as a combination of 1000 different patients undergoing immunotherapy treatment with the aid of some kind of immunosuppressive drug inhibiting Treg activity. As shown in Figure 3.8, the model simulations have sufficient variability to be partitioned with each of our clinical treatment outcome definitions. The first column of Figure 3.8 represents the change in tumor burden dynamics as Treg effectivity increases from top to bottom (primary-solid blue and metastatic dashed-red). In the second column, the most obvious variability exists in the lymphatic dendritic cell population (solid-black). In the best case (clearance), lymphatic dendritic cells saturate the lymph nodes for the majority of the simulated study period.

Ultimately, clinical treatment outcome appears to be most strongly correlated with CTL dynamics shown in the third column. There is an obvious decline in active CTL load (solid-red) from top to bottom. An important thing to note is that active CTL load is much

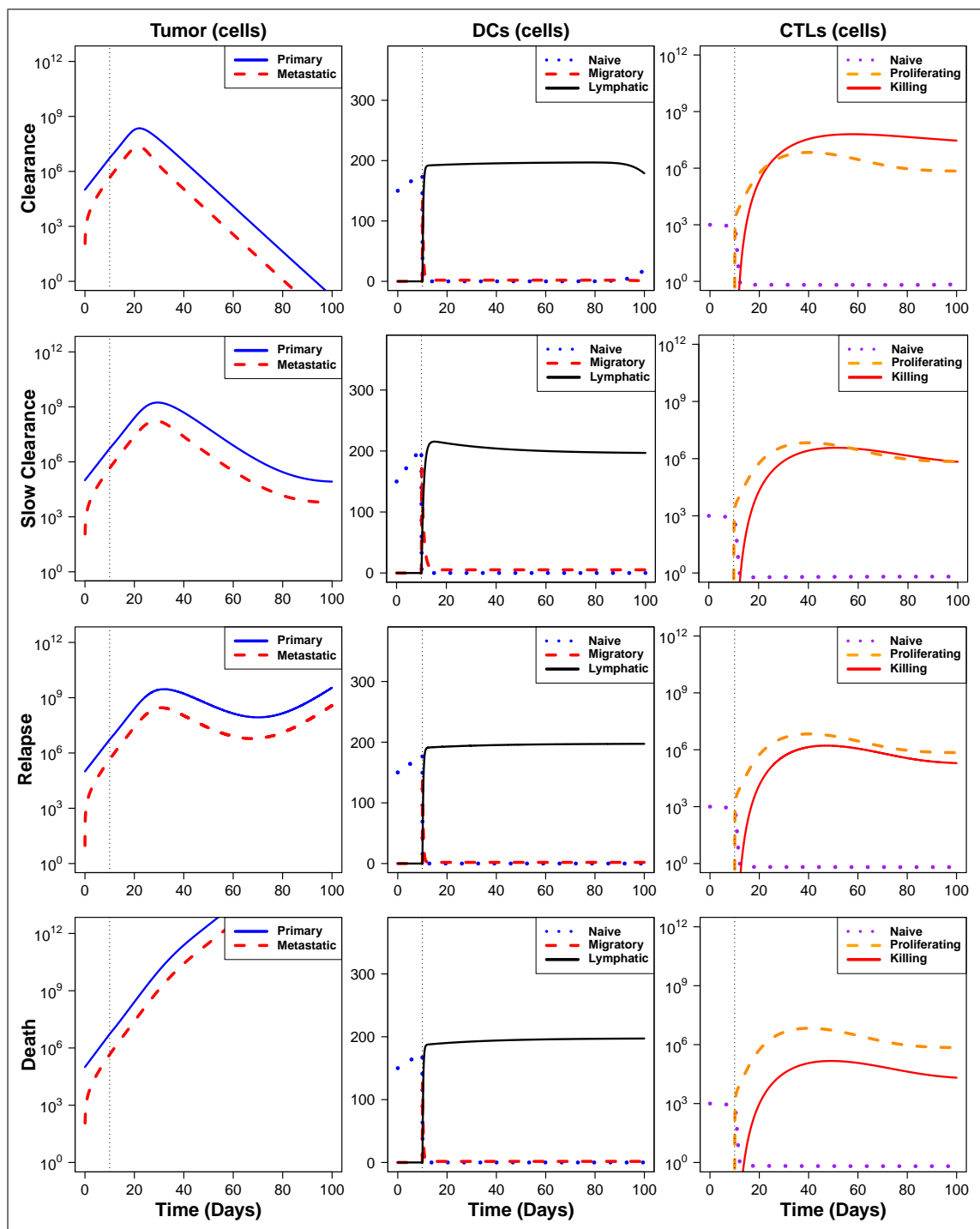


Figure 3.8. For each clinical outcome (corresponding to figure rows) defined by tumor dynamics, simulations for each cell type are shown. This figure demonstrates how clinical outcome is highly correlated with the maintenance of CTLs throughout the simulated treatment. This indirectly indicates that clinical outcome becomes more favorable as Tregs become less effective in killing CTLs. Horizontal axes represent time in days.

lower than proliferative stage CTL load (dashed-orange). This is an indication that Tregs are either killing active CTLs most efficiently or interfering with proliferation in the last row of Figure 3.8. Dynamics of all cells are driven by the complex combination of all Treg activities, which can be accounted for with changes to Treg parameters (δ_{D_0} , k , ε_A , and η).

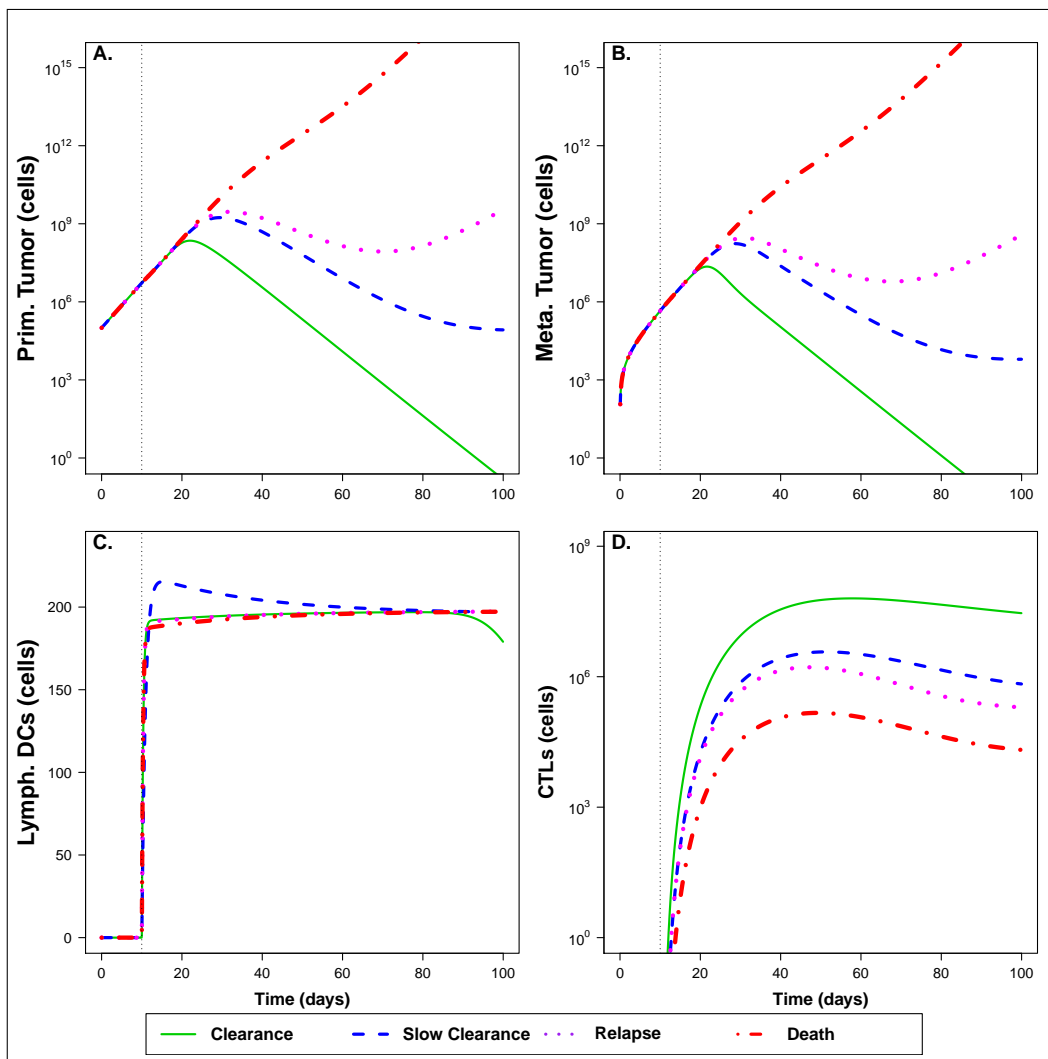


Figure 3.9. Depiction of changes in cellular dynamics as Treg activity changes. In each panel, the clinical outcome of clearance (i.e., patient survival) is in solid green, the clinical outcome of slow clearance (prolonged survival) is in dashed blue curve, the clinical outcome of relapse (possible prolonged survival) is in dotted purple, and the clinical outcome of death is in dotted-dashed red.

Figure 3.9 shows each clinical outcome for selected cells on the same plot. Primary tumor dynamics are given in Figure 3.9(A) with the clearance (solid green), slow clearance (dashed

blue), relapse (dotted purple), and death (dashed and dotted red). Results are similar in Figure 3.9(B), but represent metastatic tumor dynamics instead. As stated previously in the discussion of Figure 3.8, the dendritic cell populations do not exhibit a large degree of sensitivity to Treg parameters. This conclusion is supported by Figure 3.9(C), which shows very little variation in lymphatic DC dynamics. The strongest correlation between the tumor dynamics, as they are clinically defined, and immune dynamics comes from Figure 3.9(D). Clearance, the ideal clinical outcome, is correlated with the highest CTL load (solid green curve). As Treg effectivity increases, CTL load decreases and tumor dynamics reflect less favorable clinical outcomes.

Based on Table 3.2, the outcomes shown in Figure 3.8 and Figure 3.9 are understandable. Naive dendritic cell death increases from clearance to death, CTL fatalities increase from clearance to death, and CTL proliferation decreases from clearance to death. Dendritic cell migration does not follow an intuitive trend since the relapse and death cases occur with the highest migration rates. However, this simply reflects the model's negligible sensitivity to changes in dendritic cell migration rates in comparison to changes in proliferation or death rates for CTLs.

Table 3.2. Changes in Treg parameters from one clinical treatment outcome to the next. δ_{D_0} is the naive DC death rate, k is the active CTL death constant, η is the migratory rate for migrating DCs, and ε_A is the proliferation factor of CTLs.

Outcome	δ_{D_0}	k	η	ε_A
Clearance	0.006218062	1.817664	2.954493	4.052652
Slow Clearance	0.006218062	4.490838	1.10697	3.138794
Relapse	0.02390397	9.126924	3.046669	3.047921
Dead	0.02635106	6.259964	3.412577	2.251934

CHAPTER 4

DISCUSSION

4.1 Summary

The interactions between dendritic cells, the complete T cell repertoire, and antibodies with cancerous tumor cells and their antigens has been modeled as a system of first order ordinary differential equations [67, 68]. However, the overall treatment/post-treatment dynamics can be captured by explicitly modeling only laser treatment, DCs, the cytotoxic T cell subset, primary and metastatic tumor cells, and tumor antigen (see Equations 2.1 and B.1).

Ultimately, in this thesis we neglected explicit treatment of helper T cells, B cells, and antibodies while achieving similar tumor dynamics. We justify the omission of such immune components based on the fact that CTL effectivity is partially a function of the activity of helper T cells and B cells. This means that a reparameterization of our reduced-equation model (Equations 2.1) accounts for the effects of helper T cells and B cells. This allows for a significant reduction in the number of unknown model parameters and allows us to experiment with the effects of implicitly modeled components through strategic reparameterization.

Analysis presented in Chapter 3 suggests that anti-tumor laser immunotherapy can be accurately simulated with models like those presented in Chapter 2. As shown in Figure 3.3, the model is capable of simulating post-treatment tumor dynamics similar to those seen experimentally [15]. Because the model parameters are biologically realistic, the model can be used for clinical treatment outcome predictions.

Systematically studying the effects of glycated chitosan and regulatory T cells with LHS leads to diverse changes in tumor burden dynamics. The clinical outcome definitions outlined in Chapter 3 allowed for partitioning of model simulations as a function of GC and Treg parameters. It is important to make clinical outcome definitions to determine how successful treatment will be for any given set of parameters or initial conditions.

Treg analysis suggests that a drug used for Treg suppression needs to primarily inhibit their ability to affect CTL death and proliferation, because clinical outcomes correlate most strongly with changes in CTL load over the course of the simulated study period (Figure 3.8). Treg effects on dendritic cells in model simulations suggest a more complex relationship between clinical outcome and DC dynamics; there is not a large degree of variability in DC dynamics between the outcome cases. GC analysis suggests that clinical outcomes may be less sensitive to changes in GC parameters than in the case for Treg parameters. However, tumor dynamics still exhibit enough variability to partition simulations with three of the defined clinical outcomes (Figure 3.6).

4.2 Suggested experiments

The analysis of anti-tumor laser immunotherapy from a modeling perspective suggests a variety of experimental treatments to be performed in the laboratory. The following list discusses a few experiments that might be useful in improving treatment efficacy.

1. Since it is possible to extract CTLs for the purpose of priming for a particular invader, one suggestion would be to pursue this possibility alongside laser treatment. The goal would be to train CTLs to attack the treated tumor cell line and build a substantial CTL load for injection into the patient. The motivation comes from the fact that early tumor infiltration is best in order to eradicate tumors. An injected population could theoretically begin attacking primary and metastatic tumors soon after treatment before a second line of activated CTLs arrives. This theory is supported by results found in Section 3.2 (Figure 3.5).
2. Train dendritic cells before re-injecting them. The ultimate goal would be to activate as many CTLs as possible, which might be enhanced through a larger number of primed dendritic cells (Figure 3.5).
3. The timing of treatment tends to be crucial to patients with aggressively growing tumors. Typically, treatments in anti-tumor laser immunotherapy are performed 7 to 10 days post-inoculation. A possible experiment might be to wait a longer period of time before treatment so that treatment efficacy could be tested in a much later stage of tumor development.
4. Since tumor dynamics seem to be most closely tied to changes in Treg parameters, it might be beneficial to try to derive a drug that either decreases the number of Tregs or

mitigates their ability to kill CTLs or affect CTL proliferation. The latter drug effect is supported by Treg analysis in Section 3.4 (Figures 3.8 and 3.9).

CHAPTER 5

FUTURE WORK

5.1 Modeling

Many tumors exhibit growth patterns that cannot be explained with a simple exponential growth model. Exponential growth is used in the current model of anti-tumor laser immunotherapy because the tumor burden data suggests this type of growth. However, we can use the model to look at this treatment for other tumor cell lines. Some tumors can be modeled with logistic growth, $rP(1 - \frac{P}{K})$. The logistic growth model includes the assumption that there is some carrying capacity K that will affect overall population dynamics. This carrying capacity is a type of ceiling for tumor growth, which is related to nutrient availability and space. It would be quite simple to substitute a logistic term into the primary and metastatic tumor equations to study other tumor types. The current model can be used to study laser immunotherapy on any tumor cell line that exhibits exponential growth. This would simply call for a reparameterization of the current model to account for differences between tumor types.

The laser-tissue interaction in anti-tumor immunotherapy is much more complex than the simple time-dependent treatment function used in the current model. In order to truly understand primary tumor cell death as a function of laser heat, it is necessary to determine how heat diffuses through a non-homogeneous tumor mass to produce cell death. This calls for an application of the heat equation. The ability to quantify tumor cell death as a function of heat shock would allow us to update the treatment function in the current model.

5.2 Experimentation

The model can easily be used to test experiments that are expensive to perform in the laboratory setting. One such experiment would be to simulate the injection of a pre-primed population of CTLs post-treatment to study how this would affect tumor dynamics. This could be done by first solving the model until simulated injection was to take place and

then using the output as the initial conditions for post-injection dynamics. The CTL initial condition would dramatically increase for the post-injection period. This could also be done for dendritic cells by changing the initial condition for DCs after simulated injection of pre-primed DCs.

As described in the previous section, the model could be reparameterized to study other exponentially growing tumor lines undergoing laser immunotherapy. For tumors that reach a carrying capacity well before the death of the patient, the logistic growth model might be more accurate. With a minor change to the primary and metastatic tumor equations, simulated laser immunotherapy treatment could be performed on tumors expected to exhibit logistic growth.

5.3 Speculation

Based on the model's sensitivity to changes in CTL dynamics, simulating the injection of pre-primed CTLs would most likely yield a more successful treatment. Theoretically, this should also be true if performed in the laboratory alongside anti-tumor laser immunotherapy.

Since the model is less sensitive to DC dynamics, one could surmise that clinical outcomes would not be as sensitive to changes in DC populations by priming DCs outside the patient. If GC primarily affects dendritic cells, this would indicate that changes in GC administration should not have extreme implications for clinical treatment outcomes. However, considering the comparison of clinical outcomes influenced by GC versus other common adjuvants shown in [16], the effects of GC may be more complex than our current understanding yields.

It may be most important to focus on methods to suppress Tregs due to the model's enhanced sensitivity to Treg parameters. If it is possible to suppress these cells in the tumor microenvironment for an extended period of time, then the model suggests that CTLs will be effective in tumor cell destruction.

APPENDIX A

IMMUNOLOGICALLY EXPANDED MODEL

In our initial model, tumors were destroyed almost instantly with the chosen parameterization. Based on the tumor burden data, this time course was not accurate. The proposed mechanism behind the model on the next page is that antibody production is essential to tumor cell destruction. This possible mechanism was suggested in [11], so we chose to extend the model based on this hypothesis.

Since B cells produce antibodies upon activation, this required modeling three stages of B cell development. However, activation of B cells requires stimulus by activated helper T cells after B cells have received antigen via dendritic cells. Therefore, we modeled helper T cells, B cells, and antibodies in order to account for a delay in tumor cell destruction. Once tumors are tagged by selective antibodies, activated CTLs can then recognize them for destruction. We also hypothesized that tumors may shed antibodies after some time, so this introduced a small amount of feedback into the model. That is, tagged tumors could be recycled back into the untagged tumor population and escape immune surveillance. This meant that only sufficient antibody concentration would ultimately lead to a successful treatment.

Upon further investigation of the antibody-induced tumor cell killing mechanism, we could not reasonably conclude that this was the model that best fit the biology. This divergence was based on several immunological facts that were previously unknown. One of which, is fact that activated CTLs only need to be primed by a specific antigen in order to effectively eradicate an invader. Evidence of this is given by studies in which CTLs are extracted and trained to attack a specific tumor cell line and then re-injected, which eventually leads to complete tumor destruction.

With new parameterization of the original model, we were able to accurately simulate what is shown in tumor burden data. This allowed us to re-adopt a smaller model that is

computationally more manageable and biologically more accurate. As before, the function $\phi(t)$ is a time-dependent treatment function that drives tumor death.

$$\begin{aligned}
\left(\begin{array}{l} \text{Naive} \\ \text{Dendritic} \end{array} \right) & \frac{dD_0}{dt} = s_d - \alpha A_c D_0 - \delta_{D_0} D_0 \\
\left(\begin{array}{l} \text{Migratory} \\ \text{Dendritic} \end{array} \right) & \frac{dD_M}{dt} = \varepsilon_M \alpha A_c D_0 - \eta D_M - \delta_{D_M} D_M \\
\left(\begin{array}{l} \text{Lymphatic} \\ \text{Dendritic} \end{array} \right) & \frac{dD_L}{dt} = \varepsilon_L \eta D_M - k_1 (\beta T_0 + b B_0 + \psi H_0) D_L - \delta_L D_L \\
\left(\begin{array}{l} \text{Naive} \\ \text{CTL} \end{array} \right) & \frac{dT_0}{dt} = s_t - \beta D_L T_0 - \delta_{T_0} T_0 \\
\left(\begin{array}{l} \text{Active} \\ \text{CTL} \end{array} \right) & \frac{dT_A}{dt} = \nu_t \beta D_L T_0 - k_2 \delta_{T_0} T_A \\
\left(\begin{array}{l} \text{Naive} \\ \text{B Cell} \end{array} \right) & \frac{dB_0}{dt} = s_b - b B_0 D_L - \delta_{B_0} B_0 \\
\left(\begin{array}{l} \text{Stimulated} \\ \text{B Cell} \end{array} \right) & \frac{dB_s}{dt} = \varepsilon_s b B_0 D_L - \tau H_A B_s - \delta_{B_s} B_s \\
\left(\begin{array}{l} \text{Plasma} \\ \text{B Cell} \end{array} \right) & \frac{dB_p}{dt} = \nu_b \tau H_A B_s - \delta_{B_p} B_p \\
\left(\begin{array}{l} \text{IgG} \\ \text{Antibody} \end{array} \right) & \frac{dG}{dt} = z B_p - \delta_G G - \theta (P_0 + M_0) G \\
\left(\begin{array}{l} \text{Naive} \\ \text{Helper T} \end{array} \right) & \frac{dH_0}{dt} = s_h - (\xi B_p + \psi D_L) H_0 - \delta H_0 H_0 \\
\left(\begin{array}{l} \text{Active} \\ \text{Helper T} \end{array} \right) & \frac{dH_A}{dt} = \nu_h (\xi B_p + \psi D_L) H_0 - \delta_{H_A} H_A \\
\left(\begin{array}{l} \text{Untagged} \\ \text{Primary} \end{array} \right) & \frac{dP_0}{dt} = (1 - \mu) \gamma_p (P_0 + \epsilon_x P_1) - (\phi(t) + \theta G + \lambda_0 T_A + \delta_p) P_0 \\
\left(\begin{array}{l} \text{Tagged} \\ \text{Primary} \end{array} \right) & \frac{dP_1}{dt} = (1 - \epsilon_x) (1 - \mu) \gamma_p P_1 + \varepsilon_G \theta G P_0 - (\lambda_1 T_A + \delta_p) P_1 \\
\left(\begin{array}{l} \text{Untagged} \\ \text{Metastatic} \end{array} \right) & \frac{dM_0}{dt} = \gamma_m (M_0 + \epsilon_x M_1) + \sigma \mu \gamma_p (P_0 + \epsilon_x P_1) - (\theta G + \lambda_0 T_A + \delta_M) M_0 \\
\left(\begin{array}{l} \text{Tagged} \\ \text{Metastatic} \end{array} \right) & \frac{dM_1}{dt} = (1 - \epsilon_x) \gamma_m M_1 + (1 - \epsilon_x) \sigma \mu \gamma_p P_1 + \varepsilon_G \theta G M_0 - (\lambda_1 T_A + \delta_M) M_1 \\
\left(\begin{array}{l} \text{Tumor} \\ \text{Antigen} \end{array} \right) & \frac{dA_c}{dt} = \rho \phi(t) P_0 + p T_A (\lambda_0 P_0 + \lambda_0 M_0 + \lambda_1 M_1 + \lambda_1 P_1) - (\omega + \alpha A_c) D_0
\end{aligned} \tag{A.1}$$

Excluding the antibody-mediated tumor cell destruction mechanism for post-treatment dynamics, we can remove all B cell, helper T cell, and antibody related equations to produce our initial model without CTL proliferation. This reduces the number of tumor cell equations that we must track for post-treatment dynamics. Essentially, four tumor cell equations in the expanded model become two equations in the reduced model.

APPENDIX B

REDUCED MODEL WITHOUT CTL PROLIFERATION

With the reduced model without CTL proliferation, we have been able to accurately predict clinical treatment outcomes as a function of GC and Treg effectivity. This model has been very useful in that it has the capacity to explain a very complex system of events taking place in anti-tumor immunotherapy, but it is also relatively small and easy to explain. Interactions, in particular CTL-tumor cell interaction, are all modeled with mass-action kinetics. However, CTL dynamics are not perfectly portrayed since overall numbers of these cells are considerably low upon activation and tumor cell killing is simply too efficient. Also, this model is quite stiff so solving can produce a large degree of numerical error. The reduced model without proliferation is given as follows:

$$\begin{aligned}
 \text{(Naive Dendr)} \quad & \frac{dD_0}{dt} = s_d - \alpha A_c D_0 - \delta_{D_0} D_0 \\
 \text{(Migratory Dendr)} \quad & \frac{dD_M}{dt} = \varepsilon_M \alpha A_c D_0 - \eta D_M - \delta_{D_M} D_M \\
 \text{(Lymphatic Dendr)} \quad & \frac{dD_L}{dt} = \varepsilon_L \eta D_M - \delta_{D_L} D_L \\
 \text{(Naive CTL)} \quad & \frac{dT_0}{dt} = s_t - \beta D_L T_0 - \delta_{T_0} T_0 \\
 \text{(Active CTL)} \quad & \frac{dT_A}{dt} = \varepsilon_A \beta D_L T_0 - k \delta_{T_0} T_A \\
 \text{(Prim Tumor)} \quad & \frac{dP}{dt} = \gamma_P P - (\mu + \phi(t) - \lambda_P T_A) P \\
 \text{(Meta Tumor)} \quad & \frac{dM}{dt} = \sigma \mu P + \gamma_M M - \lambda_M T_A M \\
 \text{(Tumor Antigen)} \quad & \frac{dA_c}{dt} = \rho \phi(t) P + p T_A (\lambda_P P + \lambda_M M) - \omega A_c - \alpha A_c D_0
 \end{aligned} \tag{B.1}$$

APPENDIX C

MODEL OF CTL PROLIFERATION

In order to model the delay in tumor cell destruction without arbitrarily changing parameters to achieve this goal, we wrote the following proliferation model for CTLs upon activation. The purpose of this was to simulate a more realistic number of CTLs after activation and to accurately capture the time course of tumor - CTL interaction. Each successive proliferative stage equation multiplies the addition from the previous proliferative stage equation by some scaling factor ε_i in order to model cellular cloning from one stage to the next. The end result is a large number of active CTLs that travels to the sites of tumors and begins attacking them.

The proliferation equations given in Equations C.1:

$$\begin{aligned}
 (1^{st} \text{ stage CTL}) \quad \frac{dT_1}{dt} &= \varepsilon_1 \beta D_L T_0 - \xi T_1 - \delta_{T_0} T_1 \\
 (2^{nd} \text{ stage CTL}) \quad \frac{dT_2}{dt} &= \varepsilon_2 \xi T_1 - \xi T_2 - \delta_{T_0} T_2 \\
 (3^{rd} \text{ stage CTL}) \quad \frac{dT_3}{dt} &= \varepsilon_3 \xi T_2 - \xi T_3 - \delta_{T_0} T_3 \\
 (4^{th} \text{ stage CTL}) \quad \frac{dT_4}{dt} &= \varepsilon_4 \xi T_3 - \xi T_4 - \delta_{T_0} T_4 \\
 (5^{th} \text{ stage CTL}) \quad \frac{dT_5}{dt} &= \varepsilon_5 \xi T_4 - \xi T_5 - \delta_{T_0} T_5 \\
 (6^{th} \text{ stage CTL}) \quad \frac{dT_6}{dt} &= \varepsilon_6 \xi T_5 - \xi T_6 - \delta_{T_0} T_6 \\
 (7^{th} \text{ stage CTL}) \quad \frac{dT_7}{dt} &= \varepsilon_7 \xi T_6 - \xi T_7 - \delta_{T_0} T_7 \\
 (8^{th} \text{ stage CTL}) \quad \frac{dT_8}{dt} &= \varepsilon_8 \xi T_7 - \xi T_8 - \delta_{T_0} T_8 \\
 (\text{Final stage CTL}) \quad \frac{dT_A}{dt} &= \varepsilon_A \xi T_8 - k \delta_{T_0} T_A
 \end{aligned} \tag{C.1}$$

A comparison between CTL dynamics with and without proliferation is given in Figure C.1. Without proliferation, CTL killing of tumor cells must be extremely efficient since the total number of CTLs at any given time is quite low. With the appropriate

parameterization and mass-action killing, we have modeled post-treatment tumor dynamics accurately with our non-proliferation model. However, this model is not the most accurate fit for the underlying immunology and can produce extensive numerical error when solving the model. Figure C.1 is plotted on a log-scale, so the difference between CTLs with proliferation vs. without is several orders of magnitude for the majority of the simulated treatment period.

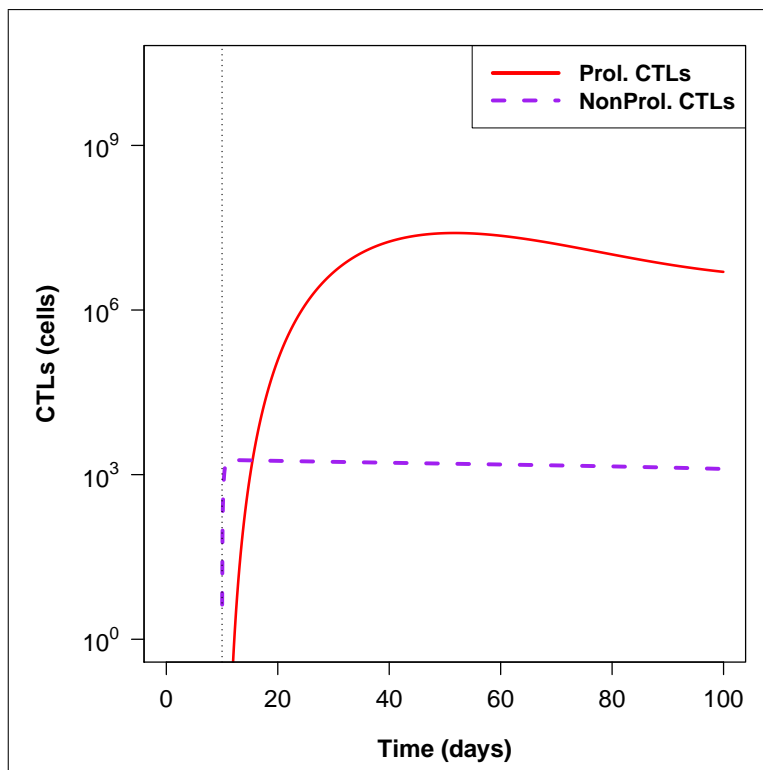


Figure C.1. Comparison of CTL dynamics with proliferation (solid-red) and without proliferation (dashed-purple). Plot is on a log scale, so overall CTL loads differ by several orders of magnitude as shown by vertical axis labels.

APPENDIX D

NON MASS-ACTION VS. MASS-ACTION TUMOR CELL KILLING

Tumor dynamics change significantly from those in model Equations B.1 by adding proliferation into the model. Since there are so many CTLs after proliferation, killing happens very quickly if modeled by mass-action. By replacing the mass-action term $\lambda_p PT_A$ by $\frac{\lambda_p PT_A}{c_p + T_A}$, we diverge from the concept of individual CTLs killing tumor cells. The latter term allows us to track tumor dynamics as a function of CTL effectivity in killing. As shown in the left panel of Figure D.1, primary tumor burden with proliferative CTLs reaches a peak later in the simulated period and decays more slowly. Similarly in the right panel of Figure D.1, metastatic tumor burden begins decaying much more slowly in the proliferative case for CTLs. This is a direct result of the non mass-action killing found in model equations 2.1.

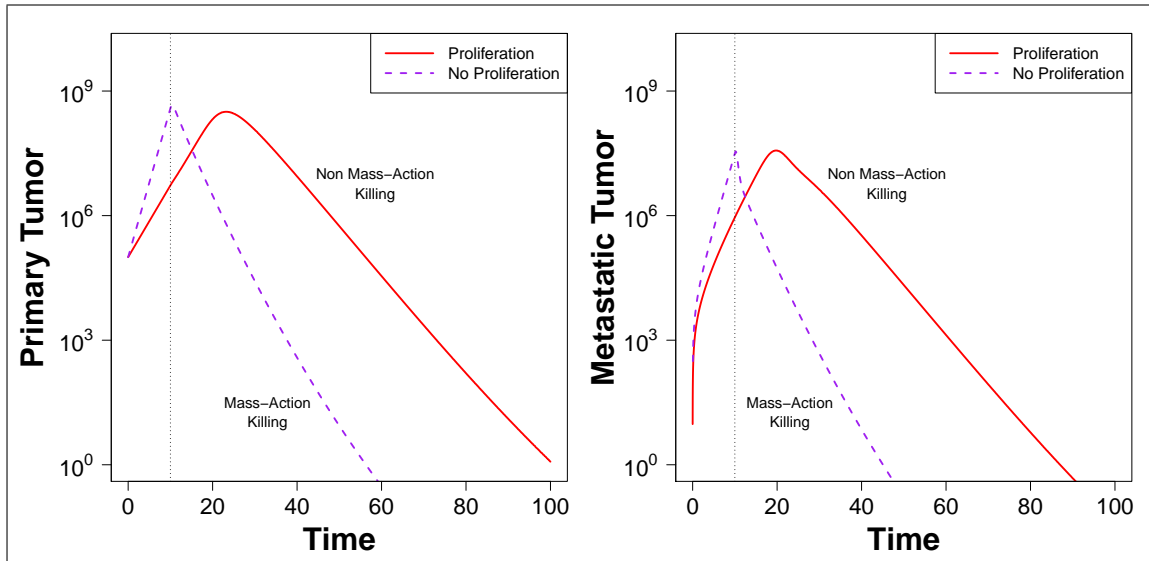


Figure D.1. Comparison of tumor dynamics with proliferation and non mass-action killing (solid-red) and without proliferation and mass-action killing (dashed-purple). **Left:** Primary tumor burdens. **Right:** Metastatic tumor burdens. Time scale is in days.

REFERENCES

- [1] Lauren Sompayrac. *How Cancer Works*. Jones and Bartlett Publishers, 2004.
- [2] Douglas Hanahan and Robert A Weinberg. The hallmarks of cancer. *Cell*, 100(1):57–70, 2000.
- [3] Douglas Hanahan and Robert A. Weinberg. Hallmarks of cancer: The next generation. *Cell*, 144(5):646–674, 2016/05/04 2011.
- [4] Lauren Sompayrac. *How the Immune System Works*. John Wiley & Sons, Ltd, 4 edition, 2012.
- [5] Steven A Rosenberg, James C Yang, and Nicholas P Restifo. Cancer immunotherapy: moving beyond current vaccines. *Nat Med.*, 10(9):909–915, September 2004.
- [6] *Immunotherapy for Lung Cancer*, volume 6 of *Proceedings of the American Thoracic Society*, 2009.
- [7] Timothy P Cripe, Pin-Yi Wang, Paola Marcato, Yonatan Y Mahller, and Patrick WK Lee. Targeting Cancer-Initiated Cells With Oncolytic Viruses. *Molecular Therapy*, 17(10):1677–1682, October 2009.
- [8] Han Hsi Wong, Nicholas R. Lemoine, and Yaohe Wang. Oncolytic Viruses for Cancer Therapy: Overcoming the Obstacles. *Viruses*, 2:78–106, January 2010.
- [9] Saleem Meerani and Yang Yao. Oncolytic Viruses in Cancer Therapy. *European Journal of Scientific Research*, 40(1), 2010.
- [10] Sanja Stevanovic, Lindsey M. Draper, Michelle M. Langhan, Tracy E. Campbell, Mei Li Kwong, John R. Wunderlich, Mark E. Dudley, James C. Yang, Richard M. Sherry, Udai S. Kammula, Nicholas P. Restifo, Steven A. Rosenberg, and Christian S. Hinrichs. Complete Regression of Metastatic Cervical Cancer After Treatment With Human Papillomavirus-Targeted Tumor-Infiltrating T Cells. *JOURNAL OF CLINICAL ONCOLOGY*, 2015.
- [11] Wei R. Chen, Robert L. Adams, Raoul Carubelli, and Robert E. Nordquist. Laser-photosensitizer assisted immunotherapy: a novel modality for cancer treatment. *Cancer Letters*, 115:25–30, 1997.
- [12] Wei R. Chen, Wei-Guo Zhu, Joseph R. Dynlacht, Hong Liu, and Robert E. Nordquist. Long-Term Tumor Resistance Induced by Laser Photo-Immunotherapy. *Int. J. Cancer*, 81:808–812, 1999.
- [13] Wei R. Chen, Anil K. Singhal, Hong Liu, and Robert E. Nordquist. Antitumor Immunity Induced by Laser Immunotherapy and Its Adoptive Transfer. *Cancer Research*, 61:459–461, 2001.

- [14] Wei R. Chen, Hong Liu, Jerry W. Ritchey, Kenneth E. Bartels, Michael D. Lucroy, and Robert E. Nordquist. Effect of Different Components of Laser Immunotherapy in Treatment of Metastatic Tumors in Rats. *Cancer Research*, 62:4295–4299, August 2002.
- [15] Wei R. Chen, Sang Won Jeong, Michael D. Lucroy, Roman F. Wolf, Eric W. Howard, Hong Liu, and Robert E. Nordquist. Induced Antitumor Immunity Against DMBA-4 Metastatic Mammary Tumors in Rats Using Laser Immunotherapy. *Int. J. Cancer*, 107:1053–1057, 2003.
- [16] Wei R. Chen, Mladen Korbelik, Kenneth E. Bartels, Hong Liu, Jinghai Sun, and Robert E. Nordquist. Enhancement of Laser Cancer Treatment by a Chitosan-Derived Immunoadjuvant. *Photochemistry and Photobiology*, 81:190–195, 2005.
- [17] M. F. Naylor, W.R. Chen, T.K. Teague, L.A. Perry, and R.E. Nordquist. In situ photoimmunotherapy: a tumour-directed treatment for melanoma. *British Journal of Dermatology*, 155:1287–1292, 2006.
- [18] Sheng Song, Feifan Zhou, Robert E. Nordquist, Raoul Carubelli, Hong Liu, and Wei R. Chen. Glycated chitosan as a new non-toxic immunological stimulant. *Immunopharmacology and Immunotoxicology*, 31:202–208, 2009.
- [19] Kathleen P. Wilkie and Philip Hahnfeldt. Tumor-Immune Dynamics Regulate in the Microenvironment Inform the Transient Nature of Immune-Induced Tumor Dormancy. *Cancer Research*, 73:3534–3544, March 2013.
- [20] Mustafa Mamat, Subiyanto Kartono, and Agus Kartono. Mathematical Model of Cancer Treatments Using Immunotherapy, Chemotherapy and Biochemotherapy. *Applied Mathematical Sciences*, 7(5):247–261, 2013.
- [21] Natalie Kronik, Yuri Kogan, Moran Elishmereni, Karin Halevi Tobias, Stanimir Vuk Pavlovic, and Zvia Agur. Predicting Outcomes of Prostate Cancer Immunotherapy by Personalized Mathematical Models. *PLoS ONE*, 5(12), December 2010.
- [22] Artem S Novozhilov, Faina S Berezovskaya, Eugene V Koonin, and Georgy P Karev. Mathematical modeling of tumor therapy with oncolytic viruses: Regimes with complete tumor elimination within the framework of deterministic models. *Biology Direct*, 1(6), February 2006.
- [23] Ralph M. Steinman. The Dendritic Cell System and Its Role in Immunogenicity. *Annual Review of Immunology*, 9:271–296, 1991.
- [24] Ralph M. Steinman and Joel Swanson. The Endocytic Activity of Dendritic Cells. *J. Exp. Med.*, 182:283–288, August 1995.
- [25] Federica Sallusto, Marina Cella, Carlo Danieli, and Antonio Lanzavecchia. Dendritic Cells Use Macropinocytosis and the Mannose Receptor to Concentrate Macromolecules in the Major Histocompatibility Complex Class II Compartment: Downregulation by Cytokines and Bacterial Products. *J. Exp. Med.*, 182:389–400, August 1995.
- [26] Ralph M. Steinman, Kayo Inaba, Shannon Turley, Philippe Pierre, and Ira Mellman. Antigen Capture, Processing, and Presentation by Dendritic Cells: Recent Cell Biological Studies. *Human Immunology*, 60:562–567, January 1999.

- [27] Peter Thumann, Isabelle Moc, Jens Humrich, Thomas G. Berger, Erwin S. Schultz, Gerold Schuler, and Lars Jenne. Antigen Loading of dendritic cells with whole tumor cell preparations. *Journal of Immunological Methods*, 277:1–16, February 2003.
- [28] Theresa L. Whiteside, Joanna Stanson, Michael R. Shurin, and Soldano Ferrone. Antigen-Processing Machinery in Human Dendritic Cells: Up-Regulation by Maturation and Down-Regulation by Tumor Cells. *The Journal of Immunology*, 173:1526–1534, 2004.
- [29] Brenda Gonzalez, Carlos Guerra, Devin Morris, Dennis Gray, and Vishwanath Venketeraman. Dendritic cells in infectious disease, hypersensitivity, and autoimmunity. *International Journal of Interferon, Cytokine and Mediator Research*, 2:137–147, November 2010.
- [30] Xiaosong Li, Tomas Hode, Maria C. Guerra, Gabriela L. Ferrel, Robert E. Nordquist, and Wei R. Chen. Laser immunotherapy for treatment of patients with advanced breast cancer and melanoma. *Journal of Physics*, 2010.
- [31] Arun T. Kamath, Sandrine Henri, Frank Battye, David F. Tough, and Ken Shortman. Developmental kinetics and lifespan of dendritic cells in mouse lymphoid organs. *Immunobiology*, 100(5):1734–1741, April 2002.
- [32] Miriam Merad and Markus G. Manz. Dendritic cell homeostasis. *Blood*, 113(15):3418–3427, April 2009.
- [33] Xinyuan Chen, Qiyuan Zeng, and Mei X. Wu. Improved efficacy of dendritic cell-based immunotherapy by cutaneous laser illumination. *Clinical Cancer Research*, 18(8):2240–2249, April 2012.
- [34] Karolina Palucka and Jacques Banchereau. Cancer immunotherapy via dendritic cells. *Nature Reviews Cancer*, 12:265–277, April 2012.
- [35] Michio Tomura, Akihiro Hata, Satoshi Matsucka, Francis H. W. Shand, Yasutaka Nakanishi, Ryoyo Ikebuchi, Satoshi Ueha, Hidekazu Tsutsui, Kayo Inaba, Kouji Matsushima, Atsushi Miyawaki, Kenji Kabashima, Takeshi Watanabe, and Osami Kanagawa. Tracking and quantification of Dendritic cell migration and antigen trafficking between the skin and lymph nodes. *Scientific Reports*, 4(6030):1–11, August 2014.
- [36] Max Schnurr, Qiyuan Chen, Amanda Shin, Weisan Chen, Tracey Toy, Corinna Jenderek, Simon Green, Lena Miloradovic, Debbie Drane, Ian D. Davis, Jose Villadangos, Ken Shortman, Eugene Maraskovsky, and Jonathan Cebon. Tumor antigen processing and presentation depend critically on dendritic cell type and the mode of antigen delivery. *Immunobiology*, 105(6):2465–2472, March 2005.
- [37] Femke Broere, Sergei G. Apasov, Michail V. Sitkovsky, and Willem van Eden. *Principles of Immunopharmacology*. Springer, 3rd edition, 2011.
- [38] Sine Hadrup, Marco Donia, and Per thor Straten. Effector CD4 and CD8 T Cells and Their Role in the Tumor Microenvironment. *Cancer Microenvironment*, 6:123–133, December 2012.

- [39] Victor Appay, Rene A. W. van Lier, Federica Sallusto, and Mario Roederer. Phenotype and Function of Human T Lymphocyte Subsets: Consensus and Issues. *Cytometry*, 73A:975–983, September 2008.
- [40] Nu Zhang and Michael J. Bevan. CD8+ T Cells: Foot Soldiers of the Immune System. *Immunity*, 35:162–168, August 2011.
- [41] Bo Wang, Christopher C. Norbury, Roberta Greenwood, Jack R. Bennink, Jonathan W. Yewdell, and Jeffrey A. Frelinger. Multiple Paths for Activation of Naive CD8+ T Cells: CD4-Independent Help. *The Journal of Immunology*, 167:1283–1289, 2001.
- [42] Shimon Sakaguchi, Tomoyuki Yamaguchi, Takashi Nomura, and Masahiro Ono. Regulatory T Cells and Immune Tolerance. *Cell*, 133:775–787, May 2008.
- [43] William L. Byrne, Kingston H.G. Mills, James A. Lederer, and Gerald C. O’Sullivan. Targeting Regulatory T Cells in Cancer. *Cancer Research*, pages 6915–6920, November 2011.
- [44] Mark J Smyth, Shin Foong Ngiow, and Michele WL Teng. Targeting regulatory T cells in tumor immunotherapy. *Immunology and Cell Biology*, 92:473–474, April 2014.
- [45] Jinfang Zhu, Hidehiro Yamane, and William E. Paul. Differentiation of Effector CD4 T Cell Populations. *Annual Review of Immunology*, 28:445–489, November 2010.
- [46] Yo-Ping Lai, Chung-Jiuan Jeng, and Shu-Ching Chen. The Roles of CD4+ T Cells in Tumor Immunity. *International Scholarly Research Network*, 2011:1–6, 2011.
- [47] Ren E.M. Toes, Ferry Ossendorp, Rienk Offringa, and Cornelis J.M. Melief. CD4 T Cells and Their Role in Antitumor Immune Responses. *The Journal of Experimental Medicine*, 189(5):753–756, March 1999.
- [48] Kenneth Hung, Robert Hayashi, Anne Lafond-Walker, Charles Lowenstein, Drew Pardoll, and Hyam Levitsky. The Central Role of CD4+ T Cells in the Antitumor Immune Response. *J. Exp. Med.*, 188(12):2357–2368, December 1998.
- [49] Yisong Y. Wan and Richard A. Flavell. How Diverse-CD4 Effector T Cells and their Functions. *Journal of Molecular Cell Biology*, 1:20–36, May 2009.
- [50] Jinfang Zhu and William E. Paul. CD4 T cells: fates, functions, and faults. *Blood*, 112(5):1557–1569, September 2008.
- [51] Alvaro Lladser, Rolf Kiessling, and C. Christian Johansson. Regulatory T Cells in Cancer. *Cancer Research*, 2010.
- [52] Ulf Petrausch, Christian H. Poehlein, Shawn M. Jensen, Chris Twitty, James A. Thompson, Ilka Assmann, Sachin Puri, Michael G. LaCelle, Tarsem Moudgil, Levi Maston, Kevin Friedman, Sarah Church, Elisa Cardenas, Daniel P. Haley, Edwin B. Walker, Emmanuel Akporiaye, Andrew D. Weinberg, Sidney Rosenheim, Todd S. Crocenzi, Hong-Ming Hu, Brendan D. Curti, Walter J. Urba, and Bernard A. Fox. Cancer Immunotherapy: The Role Regulatory T Cells Play and What can be Done to Overcome Their Inhibitory Effects. *Curr Mol Med.*, 9(6):673–682, August 2009.

- [53] Feifan Zhou, Sheng Song, Wei R. Chen, and Da Xing. Immunostimulatory properties of glycosylated chitosan. *Journal of X-Ray Science and Technology*, 19:285–292, 2011.
- [54] Assaf Marcus, Benjamin G. Gowen, Thornton W. Thompson, Alexandre Iannello, Michele Ardolino, Weiwen Deng, Lin Wang, Nataliya Shifrin, and David H. Raulet. Recognition of tumors by the innate immune system and natural killer cells. *Adv Immunol.*, 122:91–128, 2014.
- [55] Alberta Di Pasquale, Scott Preiss, Fernanda Tavares Da Silva, and Nathalie Garcon. Vaccine Adjuvants: from 1920 to 2015 and Beyond. *Vaccines*, 3:320–343, April 2015.
- [56] Xiaosong Li, Min Min, Nan Du, Ying Gu, Tomas Hode, Mark Naylor, Dianjun Chen, Robert E. Nordquist, and Wei R. Chen. Chitin, Chitosan, and Glycosylated Chitosan Regulate Immune Responses: The Novel Adjuvants for Cancer Vaccine. *Clinical and Developmental Immunology*, 2013(387023), 2013.
- [57] Anton Zilman, Vitaly V. Ganusov, and Alan S. Perelson. Stochastic Models of Lymphocyte Proliferation and Death. *PLoS ONE*, 5(9), September 2010.
- [58] Isabelle Cremer, Marie-Caroline Dieu-Nosjean, Sylvie Marechal, Colette Dezutter-Dambuyant, Sarah Goddard, David Adams, Nathalie Winter, Christine Menetrier-Caux, Catherine Sautes-Fridman, Wolf H. Fridman, and Chris G. F. Mueller. Long-lived immature dendritic cells mediated by TRANCE-RANK interaction. *Blood*, 100(10):3646–3654, November 2002.
- [59] M. McDonagh and E. B. Bell. The survival and turnover of mature and immature CD8 T cells. *Immunology*, 84, 1995.
- [60] Kaja Murali-Krishna, John D. Altman, M. Suresh, David J. D. Sourdive, Allan J. Zajac, Joseph D. Miller, Jill Slansky, and Rafi Ahmed. Counting Antigen-Specific CD8 T Cells: A Reevaluation of Bystander Activation During Viral Infection. *Immunity*, 8:177–187, February 1998.
- [61] M. D. McKay, R. J. Beckman, and W. J. Conover. A comparison of three methods for selecting values of input variables in the analysis of output from a computer code. *Technometrics*, 42(1):55–61, February 2000.
- [62] S.M. Blower and H. Dowlatabadi. Sensitivity and Uncertainty Analysis of Complex Models of Disease Transmission: an HIV Model, as an Example. *International Statistical Review*, 62(2), 1994.
- [63] R Core Team. *R: A Language and Environment for Statistical Computing*. R Foundation for Statistical Computing, Vienna, Austria, 2016.
- [64] Rob Carnell. *lhs: Latin Hypercube Samples*, 2012. R package version 0.10.
- [65] Karline Soetaert, Thomas Petzoldt, and R. Woodrow Setzer. *Solving Differential Equations in R: Package deSolve*, 2010.
- [66] Teena Mohan, Priyanka Verma, and D. Nageswara Rao. Novel adjuvants & delivery vehicles for vaccine development: A road ahead. *Indian Journal of Medical Research*, 138(5):779–795, 2013.

- [67] Sean M. Lavery, Bryan A. Dawkins, and Wei R. Chen. Laser immunotherapy and the tumor-immune system interaction: a mathematical model and analysis. *Biophotonics and Immune Responses IX*, SPIE 8944(894409), February 2014.
- [68] Bryan A. Dawkins and Sean M. Lavery. A mathematical model of the dynamics of antitumor laser immunotherapy. *Biophotonics and Immune Responses IX*, SPIE 8944(89440W), February 2014.